PHYSICAL REVIEW D **96,** 094025 (2017)

Shear viscosity of two-flavor inhomogenous color superconducting quark matter

Sreemoyee Sarkar[1,2,*] and Rishi Sharma[1,†]

[1]*TIFR, Homi Bhabha Road, Navy Nagar, Mumbai 400005, India*
[2]*UM-DAE Centre for Excellence in Basic Sciences Health Centre, University of Mumbai, Vidyanagari Campus, Kalina, Santacruz (East), Mumbai 400098, India*

(Received 13 January 2017; published 28 November 2017)

We present the first calculation of the shear viscosity for two-flavor plane wave (FF) color superconducting quark matter. This is a member of the family of crystalline color superconducting phases of dense quark matter that may be present in the cores of neutron stars. The paired quarks in the FF phase feature gapless excitations on surfaces of crescent-shaped blocking regions in momentum space and participate in transport. We calculate their contribution to the shear viscosity. We also note that the transverse t^1, t^2, t^3 gluons which are undamped in the 2SC lead to dynamic screening in the FF phase. The exchange of these gluons is the most important mechanism of the scattering of the paired quarks. We find that the shear viscosity of the paired quarks is roughly a factor of 100 smaller compared to the shear viscosity of unpaired quark matter even though their spectrum is ungapped. Therefore in the two-flavor FF phase, the unpaired quarks and the electrons give the shear viscosity of the two-flavor FF phase to a very good approximation. Our results may have implications for the damping of r-modes in rapidly rotating, cold neutron stars.

DOI: 10.1103/PhysRevD.96.094025

I. INTRODUCTION

Characterizing the nature of the phases of matter in neutron stars requires constraints on the equation of state as well as observational constraints on its transport properties. These observations help to eliminate models of dense matter inconsistent with the data. (See Refs. [1–5] for reviews.) Transport properties are sensitive to the spectrum of excitations above the equilibrium state [which is essentially the ground state because the temperatures (T) of neutron stars are much smaller than the other relevant energy scales]. These excitations can differ substantially for phases with similar equations of state.

A well-studied transport property of dense matter is the viscosity [the shear viscosity (η) and the bulk viscosity], which is connected to the spin-down rates of fast rotating neutron stars [6]. In the absence of viscous damping, the fluid in rotating neutron stars is [7,8] unstable to r-modes that lead to a rapid slow down of the neutron star rotation. Viscosities prevent the growth of r-modes. At any given temperature T, the neutron star frequency should be below a maximum [6] determined by the shear and bulk viscosities at that temperature. The shear viscosity dominates at smaller T and the bulk viscosity at larger temperatures, and the crossover point depends on the phase of dense matter. The connection between the viscosity and the spin observables is simplest if r-modes do not saturate at very small amplitudes [9,10] (determined by nonlinear physics).

Assuming there are no other damping mechanisms and that r-modes do not saturate at unnaturally small amplitudes, fluids in neutron stars [11,12] made up of only neutrons, protons and electrons do not have sufficient viscosity to damp r-modes in many rapidly rotating neutron stars [6,13–15]. Large damping at the crust-core interface [14,16,17] could stabilize r-modes in such stars, but would require unnaturally large shear viscosity for hadronic matter [18] and may not be sufficient even for extremely favorable assumptions about this contribution [6]. Appearance of various condensates and strange particles like hyperons could enhance the viscosity of the hadronic phase. This is a very active field of research [19–27]. In this context it is natural to ask if phases featuring deconfined quark matter can provide adequate damping of r-modes.

Viscosities of unpaired quark matter have been extensively analyzed in the literature [28,29]. They are dominated by excitations of quarks near their Fermi surfaces and are efficient at transport due to the large density of states of low energy excitations. Models of neutron stars featuring a core of unpaired quarks [6,15] are consistent with the observations of their rotation frequencies. (Interactions between quarks might play an important role [30] in this agreement.)

However, quarks in the cores of neutron stars are likely to be in a paired phase (see Refs. [31–33] for reviews). Pairing affects the spectrum of quasiparticles and can change the transport properties qualitatively. For example, at asymptotically high density, quark matter exists in the color flavor locked (CFL) phase [34]. All the fermionic

*sreemoyee.sinp@gmail.com
†rishi@theory.tifr.res.in

excitations in this phase are gapped and transport is carried out by Goldstone modes. The shear viscosity of the Goldstone mode associated with $U(1)_B$ breaking was calculated in [35,36]. A star made only of CFL matter is not consistent with the observed rotational frequencies [35,37], but in a star featuring a core of CFL surrounded by hadronic matter (hybrid neutron star) some mechanism involving dynamics at the interface (analogous to the one discussed in Ref. [38]) might be able to saturate r-mode amplitudes at a level consistent with observations.

At intermediate densities, the nature of the pairing pattern of quark matter is not known [33]. One exciting possibility is that the quarks form a crystalline color superconductor [39]. (See Ref. [40] for a recent review.) These phases are well motivated ground states for quark matter at intermediate densities [41–43] although their analysis is challenging because the condensate is position dependent [44]. (If the fermion coupling is strong the 2SC phase [45,46] may be favored over crystalline color superconductors [47].) Phases with gap parameters having periodic modulation in space were first proposed by Fulde, Ferrell (FF) [48], Larkin, and Ovcinnikov (LO) [49] in condensed matter systems, and phases with such pairing are commonly known as LOFF phases. In the FF phase the gap parameter is characterized by a condensate that can be written as a single plane wave. Therefore it is a simpler special case of LOFF phases for which the condensate can be written as a sum of multiple plane waves.

The LOFF phases have unique properties. They are superfluid but also have a large shear modulus [50] which can sustain quadrupole deformations in rotating neutron stars and lead to the generation of gravitational waves [51–53]. In addition, unlike the CFL phase, LOFF phases feature gapless fermionic excitations. Therefore, we expect transport properties of these phases to resemble that of unpaired quark matter.

Neutrino emission in the crystalline color superconducting phases for the simplest three-flavor condensate was computed in Ref. [54]. Stars featuring these phases in the core do indeed cool rapidly [54,55].

In this paper we present the first calculation of the shear viscosity of the simplest member of the crystalline color superconducting phases: the two-flavor FF [48] phase. The shear viscosity depends on the spectrum of the low energy modes as well as their strong interactions. Hence it is different from the neutrino emissivity where the strong interactions between quasiparticles do not play a role.

In the two-flavor FF phase (just like the isotropic 2SC phase [45,46]), the "blue" (b) colored up (u) and the down (d) quarks do not participate in pairing. Their transport properties were analyzed in Ref. [56]. But because of the presence of gapless modes (unlike the 2SC phase), the "red" (r) and the "green" (g) colored u and d quarks also contribute to the viscosity.

We argue that $ur - dg - ug - dr$ quarks scatter dominantly via exchange of the transverse t^1, t^2, and t^3 gluons (for details see Sec. III D). These gluons are Landau damped whereas in the 2SC phase the longitudinal and the transverse t^1, t^2, and t^3 gluons are neither screened nor Landau damped [57–60]. The polarization tensors of the t^1, t^2, and t^3 gluons are anisotropic [61].

Therefore, both the quasiparticle dispersions and their interactions are anisotropic, and the usual techniques to simplify the collision integral in the Boltzmann equation [29] are not applicable, making its evaluation challenging. Furthermore, the Boltzmann analysis needs to be modified to accommodate the fact that the excitations are Bogoliubov quasiparticles. To address this we find it convenient to separate the modes in the two Bogoliubov branches [Eq. (25)] into modes [Eq. (26)] corresponding to momenta ($|\mathbf{p}|$) greater than the chemical potential (μ) (in the absence of pairing these are associated with particle states) and $|\mathbf{p}| < \mu$ (in the absence of pairing these are associated with hole states). This makes the formalism a multispecies problem.

Quasiparticle modes near the gapless surface dominate transport, but the shape of the surface of the gapless surface in the FF phase is nontrivial. In addition, the momentum transferred between the quasiparticles can be large and a small momentum expansion cannot always be made. Therefore we evaluate the collision integral [Eq. (11)] numerically.

The main result of the computation is given in Eq. (60) and in Fig. 6. The central conclusion is that the viscosity of the $ur - dg - ug - dr$ quarks is reduced compared to their contribution in unpaired quark matter by a factor of roughly 100. The detailed analyses and the dependence of the shear viscosity on T and the splitting between the Fermi surfaces $\delta\mu$ are shown in Sec. IV B.

The reduction of the viscosity by a large factor depends on the properties of the mediators between the quasiparticles. For example, if we use the Debye screened longitudinal gluons (this is appropriate for one-flavor FF pairing and is also a good model for condensed matter systems like the FF phase in cold atoms), then the viscosity of the paired fermions remains unchanged from its value in the absence of pairing. This is because, the geometric factors associated with the reduced area of the Fermi surface cancel out. (See Sec. IV A for details.) We give an intuitive argument to clarify the difference between long-ranged and short-ranged interactions. These results (Sec. IV A), though not directly relevant for the two-flavor FF phase, provide intuition for the three-flavor crystalline phases where both the longitudinal and the transverse gluons are screened, and may also be relevant for condensed matter systems where the transverse gauge bosons do not play a role.

To understand some aspects of the numerical results obtained for the FF phase (Sec. IV) we use our formalism to calculate the viscosity in isotropically paired systems with Fermi surface splitting in Appendix E. For these systems it is possible to compare the numerical results with simple

analytic expressions in certain limits. The results of Appendix E are not novel, but clarify some physical aspects of the problem. For example we study the role played by the scattering of paired fermions with phonons in suppressing their transport which has not been highlighted before. While the role played by phonon-fermion scattering is only of academic importance in the extreme limits $\Delta \gg T$ and $\Delta \ll T$, it may be important in the intermediate regime where $\Delta > T$ but not $\Delta \gg T$.

The plan of the paper is as follows. We quickly review the basics of the FF phase in Sec. II and compare the low energy excitations in this phase to unpaired quark matter and the CFL phase. In Sec. III we set up the problem. The basic formalism is the multicomponent Boltzmann transport equation (Sec. III A) which we solve in the relaxation time approximation. We describe the low energy modes in Secs. III B and III C and their interactions in Sec. III D.

In Sec. IV we show results for the FF phase. We compute the shear viscosity in the FF phase for a simple interaction given in Eq. (47) in Sec. IV A. We give the results for the t^1, t^2, t^3 interaction in Sec. IV B. We summarize the results and speculate about some implications for neutron star phenomenology in Sec. V.

Description of the relevant FF phase space (Appendix A), detailed steps to evaluate the collision integral (Appendix B), a quick review of the effective Lagrangian for the two-flavor pairing (Appendix C), clarifications of the role played by the phonons (Appendix D), results for the isotropic pairing (Appendix E) and the details about the numerical implementation of the collision integrals (Appendix F) are given in the appendix.

II. REVIEW

To set up the Boltzmann transport equation for the crystalline phase we need to understand the excitation spectra and the interactions between the quasiparticles. This requires the understanding of the symmetry breaking pattern of the crystalline phases which we review here. Experts in the field can skip to the end of the section and start from Sec. III A.

A benchmark quark matter phase to compare and contrast the properties of paired quark matter is unpaired quark matter. In the absence of pairing, the excitation spectrum is simply

$$E = |\xi| = ||\mathbf{p}| - \mu| \tag{1}$$

where $\xi = |\mathbf{p}| - \mu$ is the radial displacement of the momentum vector from the Fermi surface. The excitations at the Fermi surface (defined by $\xi = 0$) are gapless and can be excited thermally; therefore fermions near the Fermi surface are very efficient at transporting momentum and charge.

The interactions between the quarks are mediated by gluons (eight gluons corresponding to the generators $t^1, \ldots t^8$[1]) and the photon. In the absence of pairing, the longitudinal components of these mediators are Debye screened [28]. The transverse components of the mediators (magnetic components) are unscreened in the presence of static fluctuations of the current, and are only dynamically screened (Landau damping). Consequently, they have a longer range compared to the longitudinal gauge bosons and dominate scattering in relativistic systems [29] at low T. This can be understood as follows. The screening mass for the longitudinal gauge bosons is given by the $m_{\text{Debye}} \sim \Pi_l^{1/2}$ where $\Pi_l \sim g\mu$ is the longitudinal polarization tensor (g is the coupling and μ is the chemical potential). On the other hand Landau damping is proportional to the energy exchange, and damping occurs on a momentum scale $m_{\text{Landau}} \sim (\omega \Pi_l)^{1/3}$ [63]. [For a concrete estimate see Eq. (E8)]. The energy exchange ω is of the order of T which is much smaller than μ for neutron stars. Consequently, the transverse gluons, if unscreened, have a longer range compared to the longitudinal gluons and therefore their exchange is the dominant scattering mechanism for the quarks. This argument will turn out to be important in Sec. IV B, when we discuss which are the most important scattering mechanisms in the FF phase.

Attractive color interactions between quarks induce Cooper pairing between quarks. At asymptotically high densities [corresponding to a quark number chemical potential μ sufficiently larger than the strange quark mass (m_s)], the strange quark mass can be ignored, and the Lagrangian is symmetric under SU(3) transformations between the up (u or 1), down (d or 2) and (s or 3) quarks. They can all be treated as massless and form Cooper pairs in a pattern that locks the color and flavor symmetries (CFL phase) [34]. The condensate is translationally invariant, which corresponds to pairing between quarks of opposite momenta.

Pairing qualitatively alters both the spectrum of quasiparticles as well as their interactions. The fermionic excitations are nine Bogoliubov quasiparticles [34] (for each handedness) which are all gapped. The scale of the gap is set by $\Delta_{0\text{CFL}}$ which is expected to be of the order of a few 10s of MeV while the temperatures of the neutron stars of interest are at most a few keV. Therefore the quarks do not participate in transport.

Since the fermions are all gapped in this phase, the low energy theory consists of the Goldstone modes ("phonons") associated with the broken global symmetries [34,64–70]. The phonons have macroscopically large mean free paths (of the order of the size of the neutron star or typical vortex separations [36]). Flow on smaller length scales compared to the mean free path then becomes dissipationless, and r-modes cannot be efficiently damped in the CFL phase for temperatures below 10^{10} K, in contradiction with the data

[1]We use the standard notation for the Gell-Mann matrices [62] as the generators of the color SU(3).

[37]. The above discussion suggests that if a quark matter core damps the r-modes, then it features gapless fermionic excitations unlike the CFL phase.

At neutron star densities the strange quark mass cannot be neglected. The strange quark mass stresses the cross-species pairing [39,71] of the CFL phases. To understand the origin of this stress, note that in the absence of pairing, the Fermi surfaces of the quarks in neutral three-flavor quark matter in weak equilibrium Refs. [39,71] are given by [72]

$$p_F^d = p_F^u + \frac{m_s^2}{4\mu}, \qquad p_F^s = p_F^u - \frac{m_s^2}{4\mu} \tag{2}$$

implying, in particular, that the splitting between the $u-d$ and the $d-s$ Fermi surfaces is

$$2\delta\mu = \frac{m_s^2}{4\mu}. \tag{3}$$

On the other hand pairing between fermions of opposite momenta is strongest if the pairing species have equal Fermi momenta. This argument suggests that when $\delta\mu \sim \Delta_{0\mathrm{CFL}}$, the symmetric pairing pattern of the CFL phase is likely to be disrupted.

The LOFF phase was proposed as the plausible ground state for stressed quark matter [39,73]. (For a review of other ways quark matter can respond to the stress on pairing see Ref. [33]). The motivation for this proposal is that a condensate of the form

$$\langle \psi_i(r)\psi_j(r)\rangle = \Theta e^{2i\mathbf{b}\cdot\mathbf{r}} \tag{4}$$

allows pairing along rings on split Fermi surfaces for $b = |\mathbf{b}| > \delta\mu$ [39][2] ($b, \delta\mu$ and Δ are all taken to be much smaller than μ). $\mathbf{b}$ defines the wave vector for the periodic variation of the condensate.

In the Nambu-Jona-Lasinio (NJL) model, it is well known that the phase with the condensate given in Eq. (4) is preferred over unpaired matter as well as the space independent condensate for $\delta\mu \in [0.707\Delta_0, 0.754\Delta_0]$ [39] where Δ_0 is the two-flavor gap for $\delta\mu = 0$.

At the upper end of this range the transition from the FF phase to the normal phase takes place. The FF phase is favored over the unpaired phase for $\delta\mu < 0.754\Delta_0$. As we increase $\delta\mu$ there is a second order phase transition from the FF to the normal phase. i.e. $\Theta \to 0$ smoothly when $\delta\mu \to 0.754\Delta_0$ from the left. The most favored momentum b near $\delta\mu = 0.754\Delta_0$ is

$$b = \zeta\delta\mu, \tag{5}$$

with $\zeta \approx 1.2$ [48,49,72,74,75]. (This number is conventionally called η in the literature but in this manuscript we give it a different symbol to avoid confusion with the viscosity η.) For plots of Δ versus $\delta\mu$ in FF-like phases please see Ref. [74,75].

At the lower end of the range the homogeneous paired phase with pairing parameter Δ_0 is favored over the FF phase for $\delta\mu < 0.707\Delta_0$. (For single gluon exchange the window of favorability is larger [76].)

Intuitively one expects [74] that condensates featuring multiple plane waves (LOFF condensates)

$$\langle \psi_i(r)\psi_j(r)\rangle = \Theta\sum_m e^{2i\mathbf{b}_m\cdot\mathbf{r}} \tag{6}$$

can pair quarks along multiple rings and give a stronger free energy benefit as long as the pairing rings do not overlap. The set of plane waves $\{\mathbf{b}_m\}$ defines a crystal structure. A detailed calculation [74] till the sixth order in the pairing parameter in the Ginzburg-Landau approximation confirms this and shows that the window of favorability of LOFF phases can be larger. A more recent sophisticated numerical analysis reveals [44] that the Ginzburg-Landau calculation might overestimate the favorability of the LOFF phases. Nevertheless, it is of interest to study a range of parameters ($\delta\mu$) where LOFF phases could be the ground state of quark matter.

Motivated by this discussion, in Sec. IV we calculate the shear viscosity of the two-flavor FF phase in the range $\delta\mu \in [0.575, 0.75]\Delta_0$. The upper limit of the range is motivated by the fact that at $0.754\Delta_0$ the gap parameter in the FF phase goes smoothly to 0 and the shear viscosity of the FF phase tends to well-known results for unpaired quark matter. The lower limit of $\delta\mu = 0.575\Delta_0$ is taken to be smaller than $0.707\Delta_0$ where homogeneous pairing wins over the FF pairing, with an eye towards the possibility that the FF calculation might capture aspects of more complicated LOFF-like phases. Therefore, this range covers a wide range of $\delta\mu$ where the LOFF phases could be the ground state of quark matter.

For the three-flavor problem, the form of the LOFF condensate [41,75,77] is

$$\langle \psi_{cfs}(r)\psi_{c'f's'}(r)\rangle = \sum_I \sum_{\{\mathbf{b}_m\}^I} \Theta_I e^{2i\mathbf{b}_m\cdot\mathbf{r}} \epsilon_{Icc'}\epsilon_{Iff'}\epsilon_{ss'}. \tag{7}$$

s, s' are the Weyl spinor indices; f are flavor indices that run from 1 to 3. c, c' are color labels that run over 1 (colloquially red or r), 2 (green or g), and 3 (blue or b). The left-handed quarks (L) and the right-handed quarks (R) pair among themselves and can be treated independently.

Within the Ginzburg-Landau approximation [41], condensates of the form Eq. (7) for two crystalline phases have a lower free energy than unpaired quark matter as well as homogeneous pairing phases over a wide range of the

[2]The real number b refers to $|\mathbf{b}|$, which is different from the blue colored quark. b as an index in the set $\{a, b, c, d\}$ refers to the branch of the dispersion as we discuss below. We apologize for the degeneracy in notation but the contexts are quite different and hence unlikely to cause confusion.

parameters μ, Δ and m_s that are expected to exist in neutron star cores [42].

Therefore it is natural to evaluate its transport properties and test whether they are consistent with existing and future observations. As mentioned above, neutrino emissivity for a three-flavor LOFF phase with the simplest three-flavor crystal structure was computed in Ref. [54].

In this paper we take the first step in the calculation of the shear viscosity in crystalline color superconductors. To simplify the calculations we ignore the s quarks completely and consider phases with a single plane wave condensate,

$$\langle \psi_{cfs}(r)\psi_{c'f's'}(r)\rangle = \Theta_3 e^{2i\mathbf{b}\cdot\mathbf{r}}\epsilon_{3cc'}\epsilon_{3ff'}\epsilon_{ss'}, \qquad (8)$$

which corresponds to taking $\Theta_1 = \Theta_2 = 0$ in Eq. (7), as well as limiting the set of momentum vectors $\{\mathbf{b}_m\}$ to just one vector $\mathbf{b}$.

Equation (8) models FF pairing between ur, dg quarks and the ug, dr quarks. The Fermi surfaces of the u and d quarks are split by $2\delta\mu = \mu_d - \mu_u$ which can be thought of as the measure of the strange quark mass $\delta\mu \sim m_s^2/(4\mu)$ if strange quarks are present (similar to the 2SC + s phase), or the electron chemical potential $\delta\mu \sim \mu_e/2$ [78] (similar to the 2SC phase) if electrons ensure neutrality.

The excitation spectrum of the paired quarks governed by the pairing parameter Δ is related to the condensate Θ by the relation $\Delta = \lambda\Theta$ where λ is proportional to the strength of the NJL interaction [34].

With condensation in only a single plane wave the dispersions of the paired fermions [39] in the FF state have a compact analytic form [Eq. (24)]. We see that even with these approximations, the calculation of the viscosity contributions of the $ur - ug - dr - dg$ quarks is nontrivial because of pairing. Geometrically, Eq. (8) represents pairing between two Fermi surfaces with radii $\mu \pm \delta\mu$ and centers displaced by $2\mathbf{b}$ (Fig. 7). For $b > \delta\mu$, the two Fermi surfaces intersect. For $\Theta_3 \to 0$ (true near the second order phase transition between the inhomogeneous and unpaired phase), the pairing parameter is small and pairing cannot occur when either the u or the d momentum state is unoccupied [39]. (See Sec. A for a quick reminder.) The boundary of these "pairing regions" features gapless fermionic excitations. This suggests that the contributions of the paired $ur - dg - ug - dr$ quarks are not very different from their contributions in unpaired quark matter.

However, the shapes of the gapless Fermi surfaces in LOFF pairing are quite complicated, and their areas drop rapidly as Θ_3 increases as we decrease $\delta\mu$ from $0.754\Delta_0$. Therefore, till now it was not clear how their contributions behave in the neutron star core. We answer this question in this paper. In addition, for a phase with condensate Eq. (8), the ub and the db quarks are unpaired. We assume here that neutrality is ensured by electrons, and the electrons are gapless and contribute to transport also. Their contributions to shear viscosity were analyzed for the 2SC phase in Refs. [56] and we show comparisons of the $ur - ug - dr - dg$ contribution to their results for the shear viscosity of the electrons and the (dominant) db quarks in Fig. 6. Finally, since the condensate depends on position, there are massless phonons associated with the breaking of spatial symmetries. We analyze their contribution in Appendix D.

We note as an aside that Eq. (8) has the same color, flavor and spin structure as the homogeneous and isotropic 2SC phase [45,46]. For weak and intermediate coupling strengths [79,80], the 2SC phase has a smaller free energy compared to the CFL phase and unpaired quark matter, only for temperatures larger than a few MeV [79–82]. For large couplings [79,80] however, 2SC phase is favored over the CFL and the unpaired phase over a range of chemical potentials expected to be present in some region in the cores of neutron stars (350 to 400 MeV). In the 2SC phase the $ur - dg - ug - dr$ quarks are paired and gapped (the gapless 2SC phase is unstable [78,83]). The low energy dynamics are therefore dominated by the unpaired ub and db quarks. Transport in this phase has been analyzed in detail in Ref. [56]. The bulk viscosity for the 2SC phase was computed in Ref. [84]. The transport properties of b quarks are similar to that in unpaired quark matter and hence we expect that viscosities should be large enough to damp r-mode instabilities if a large volume of 2SC matter is present in the cores of neutron stars. Therefore, the occurrence of this phase may provide a plausible mechanism for the damping of r-modes. For intermediate and weak coupling the crystalline phases are well motivated candidate phases at neutron star densities.

In addition to the spectrum of excitations, the collision integral requires knowledge about the interactions between the quasiparticles in the FF phase. The condensate of the form Eq. (8) leaves a SU(2) subgroup of color associated with $r - g$ quarks unbroken. Therefore, the t^1, t^2, t^3 gluons do not pick up a Meissner mass [57,58]. As we see, because of this, the t^1, t^2, t^3 gluons play a special role in the two-flavor FF phase that we consider. The color transformations corresponding to the $t^4 \ldots t^7$ generators are broken and the associated transverse gauge fields do develop a Meissner mass. The longitudinal components of the $t^4 \ldots t^7$ gauge fields are Debye screened [58,60]. Similarly, the t^8 gluons feature Meissner and Debye screening [58,60]. Finally, as in the case of the CFL phase, the transverse components of a linear combination of t^8 and Q gauge bosons ($\tilde{Q}$ photon) have vanishing Meissner mass.

This discussion motivates our analysis of viscosity in the FF phases. In the following section we develop the formalism to calculate the shear viscosity coefficient in this crystalline phase.

III. FORMALISM

This section develops the theoretical aspects of the calculation of transport coefficients in the LOFF phase.

We start our discussion with the Boltzmann equation in an anisotropic system.

A. Boltzmann transport equation

In a system of multiple species, the relaxation times τ_i for the species i can be found by solving a matrix equation,

$$L_i^{(n)} = \sum_j [R_{ij}^{(n)}]\tau_j^{(n)}. \tag{9}$$

The above equation is the Boltzmann equation for a multispecies problem, where L_i is the left-hand side (lhs) and $[R_{ij}]$ is the right-hand side (rhs) of the equation. L_i can also be related to the phase space of quasiparticles that participate in transport, and $[R_{ij}]$ as the collision integral. We have labeled the collisional integral with an additional index (n) associated with the tensor structure of the transport property we are considering.

To be concrete, consider a situation where transport is dominated by fermionic particles and their interaction with each other provides the most important scattering mechanism. As was shown in Ref. [56] for multiple quark species (the single species Boltzmann transport equation for quarks has been studied since Ref. [85]) the lhs and rhs of the Boltzmann transport equation for each species i can be written as

$$L_i^{(n)} = \frac{1}{\gamma^{(n)}} \int \frac{d^3p_i}{(2\pi)^3} \frac{df_0^i}{d\epsilon} (\phi_i^{ab}\psi_i^{ab}) \tag{10}$$

and

$$\begin{aligned}\sum_j [R_{ij}^{(n)}]\tau_j^{(n)} = &-\sum_{j_2 j_3 j_4} \frac{\nu_2}{T\gamma^{(n)}} \int \frac{d^3p_i}{(2\pi)^3}\frac{d^3p_2}{(2\pi)^3}\frac{d^3p_3}{(2\pi)^3}\frac{d^3p_4}{(2\pi)^3} \\ &\times \overline{|\mathcal{M}|^2}(ij_2 \to j_3 j_4) \\ &\times (2\pi)^4 \delta\left(\sum p^\mu\right)[f_i f_2 (1-f_3)(1-f_4)] \\ &\times 3\phi_i.[\tau_i^{(n)}\psi_i^{(n)} + \tau_{j_2}^{(n)}\psi_{j_2}^{(n)} - \tau_{j_3}^{(n)}\psi_{j_3}^{(n)} - \tau_{j_4}^{(n)}\psi_{j_4}^{(n)}].\end{aligned} \tag{11}$$

In the above equations f is the Fermi-Dirac distribution function and ν_2 is the degeneracy factor for species j_2. In the cases we consider the degeneracy is associated with spin and the degeneracy factor is 2. $\mathcal{M}(ij_2 \to j_3 j_4)$ refers to the transition matrix element for the scattering of the initial states featuring particles of species i, and j_2 (which have momenta p_i, p_2 respectively) to the final species j_3, j_4 (which have momenta p_3, p_4 respectively). For a fixed species i, the sum over j_2, j_3, and j_4 in Eq. (11) runs over all the species in the multispecies formalism. The main new feature compared to the multispecies Boltzmann transport derived in Ref. [56] arises in our problem because of pairing, which gives rise to a doubling of degrees of freedom as described below in Eq. (26).

In Eq. (11) we have assumed that all the species participating in scattering are fermionic. If gluon/phonon radiation or absorption is important then their contributions have to be added in the collision integral in Eq. (11) with appropriate changes from fermionic to bosonic distribution functions [see Eq. (D3) for example].

In this system fermion scattering is dominant. In Sec. D 1 we show that processes involving quark scattering with phonons are subdominant in gapless phases. Absorption and emission of screened gauge bosons is exponentially suppressed by the factor $\exp(-m_{\text{screen}}/T)$ where m_{screen} is the screening mass. Finally for massless gauge bosons these processes are forbidden because they do not satisfy energy and momentum conservation simultaneously. While number changing processes $2 \Rightarrow 3$ like $f_i + f_2 \Rightarrow f_3 + f_4 + b$ can contribute, they occur at higher order in the coupling constants and hence are typically ignored.

The form of the flows ϕ and ψ in Eq. (11), relevant for the calculation of the shear viscosity, is given by

$$\begin{aligned}\phi_i^{ab} &= p^a v^b, \\ \psi_i^{ab} &= \Pi^{(n)ab\alpha\beta}\phi_i^{ab},\end{aligned} \tag{12}$$

where

$$v^a = \frac{dE}{dp^a}. \tag{13}$$

$\Pi^{(n)ab\alpha\beta}$ are the operators that project the shear viscosity tensor into a number of subspaces, (n), invariant under the rotational symmetries of the system. The γ^n, defined by

$$\gamma^{(n)} = \Pi^{(n)ab\alpha\beta}\delta^{a\alpha}\delta^{b\beta}, \tag{14}$$

are the dimensions of these subspaces.

For example, in an isotropic system, the shear viscosity tensor should be invariant under all rotations, and the only projection operator is the traceless symmetric tensor

$$\Pi^{ab\alpha\beta} = \left(\frac{1}{2}\delta^{a\alpha}\delta^{b\beta} + \frac{1}{2}\delta^{a\beta}\delta^{b\alpha} - \frac{1}{3}\delta^{ab}\delta^{\alpha\beta}\right), \tag{15}$$

with $\gamma = 5$.

We consider a system where the condensate chooses a particular direction and such systems have five independent forms. In particular, we focus on $n = 0$ for which

$$\begin{aligned}\Pi^{(0)} &= \left(\frac{3}{2}\right)\left(b_a b_b - \frac{1}{3}\delta_{ab}\right)\left(b_\alpha b_\beta - \frac{1}{3}\delta_{\alpha\beta}\right) \\ \gamma^{(0)} &= 1.\end{aligned} \tag{16}$$

The contribution to the viscosity tensor for each species i is given by

$$\eta_i^{ab\alpha\beta} = \sum_{(n)} \eta_i^{(n)} \Pi^{(n)ab\alpha\beta}, \tag{17}$$

where

$$\eta_i^{(n)} = \left(-\frac{3}{2}\gamma^{(n)}\nu_i\right)[L_i^{(n)}]\tau_i^{(n)}, \tag{18}$$

where ν_i is the degeneracy factor for the ith species.

To evaluate both Eqs. (10) and (11) we need to identify the relevant species, the interactions between them as well as the phase space in which the relevant scatterings occur. We explain these in the next sections. A detailed discussion of the collision kernel required to perform numerical analysis has been presented in Appendix B.

B. Quark species

We consider phases with a condensate of the form

$$\langle \psi_{cfs}(r)\psi_{c'f's'}(r)\rangle = \Theta_3(r)\epsilon_{3cc'}\epsilon_{3ff'}\epsilon_{ss'}. \tag{19}$$

We ignore the contribution of the s quarks which, if present (2SC + s phase [78]), are unpaired. Only $ur - dg$ and $ug - dr$ quark pairs participate in pairing. The ub and db (b color) quarks as well as the electrons are unpaired.

Transport affected by the ub and the db quarks, as well as by the electrons in the homogeneous and isotropic 2SC phase, has been studied in detail in Ref. [56]. Since they are unpaired, techniques from condensed matter theory for calculating transport in Fermi liquids can be used to simplify the calculation, although there are new features associated with the fact that the quarks are relativistic [63] and due to the nontrivial color and flavor structure of the interaction [56].

Here we focus on the effect of crystalline pairing on quark transport. In the full three-flavor theory with $\Theta_1, \Theta_2 \neq 0$, the ub and db species as well as the strange quarks participate in crystalline pairing [Eq. (7)]. Therefore we need to develop techniques to calculate fermionic transport properties in the presence of a crystalline order parameter. In this paper, we limit ourselves to the calculation of transport in the two-color two-flavor subsystem of $ur - dg - ug - dr$ quarks. Even in this two-color, two-flavor subspace, the theory of transport is quite rich and we learn valuable lessons that will help in future attempts to extend the calculations to the three-flavor problem.

C. Spectrum of excitations

The most important input required to evaluate the transport coefficients in the FF phase is the anisotropic quasiparticle dispersion relation. To obtain the dispersion relations for the $ur - dg - ug - dr$ quarks we diagonalize the mean field Lagrangian. Details of the mean field Lagrangian can be found in Appendix C.

The energy eigenvalues for quasiparticles in the $ur - dg$ sector are the eigenvalues of the following matrix,

$$\begin{pmatrix} (E - |\mathbf{p}+\mathbf{b}|) + \mu_u & -\Delta \\ -\Delta^* & (E + |\mathbf{p}-\mathbf{b}|) - \mu_d \end{pmatrix}. \tag{20}$$

The corresponding matrix for the $ug - dr$ sector is identical and the $ug - dr$ sector can be handled in an identical fashion.

The eigenvalues and the eigenvectors are given by

$$E_1 = (|\mathbf{p}+\mathbf{b}| - |\mathbf{p}-\mathbf{b}| + 2\delta\mu)/2 - \sqrt{\xi^2+\Delta^2},$$
$$\mathbf{u}_1 = \begin{pmatrix}\Phi_{11}\\ \Phi_{12}\end{pmatrix} = \begin{pmatrix} \frac{1}{\sqrt{2}}\sqrt{1-\frac{\xi}{\epsilon}} \\ -e^{-i\phi}\frac{1}{\sqrt{2}}\sqrt{1+\frac{\xi}{\epsilon}}\end{pmatrix} \tag{21}$$

and

$$E_2 = (|\mathbf{p}+\mathbf{b}| - |\mathbf{p}-\mathbf{b}| + 2\delta\mu)/2 + \sqrt{\xi^2+\Delta^2},$$
$$\mathbf{u}_2 = \begin{pmatrix}\Phi_{21}\\ \Phi_{22}\end{pmatrix} = \begin{pmatrix} \frac{1}{\sqrt{2}}\sqrt{1+\frac{\xi}{\epsilon}} \\ e^{-i\phi}\frac{1}{\sqrt{2}}\sqrt{1-\frac{\xi}{\epsilon}}\end{pmatrix} \tag{22}$$

where, $\xi = (|\mathbf{p}+\mathbf{b}| + |\mathbf{p}-\mathbf{b}| - 2\mu)/2$, $\epsilon = \sqrt{\xi^2+\Delta^2}$ and ϕ is the phase of Δ.$\mu = (\mu_u + \mu_d)/2$ is the mean of the chemical potentials and $\mu_d - \mu_u = 2\delta\mu$.

The Bogoliubov coefficients can be arranged in an orthonormal matrix form,

$$[\Phi] = \begin{pmatrix}\Phi_{11} & \Phi_{21}\\ \Phi_{12} & \Phi_{22}\end{pmatrix} = (\mathbf{u}_1\mathbf{u}_2). \tag{23}$$

In the limit $\mu \gg \delta\mu, b, \Delta$, and $\mu \gg T$, the energy eigenvalues can be approximated with the help of the Fermi liquid approximation, i.e. only scatterings near the Fermi surface are relevant. With these approximations the energy eigenvalues become

$$E_1(\mathbf{p}) = \delta\mu + \mathbf{b}\cdot\mathbf{v}_F - \sqrt{\xi^2+\Delta^2},$$
$$E_2(\mathbf{p}) = \delta\mu + \mathbf{b}\cdot\mathbf{v}_F + \sqrt{\xi^2+\Delta^2}, \tag{24}$$

or in polar coordinates with $\hat{b} = \hat{z}$,

$$E_1(\xi,\theta) = \delta\mu + b\cos\theta - \sqrt{\xi^2+\Delta^2},$$
$$E_2(\xi,\theta) = \delta\mu + b\cos\theta + \sqrt{\xi^2+\Delta^2}, \tag{25}$$

where $\xi = p - \mu$ and $\mathbf{v}_F = (d\xi/dp)\hat{p} = \hat{p}$ is the Fermi velocity.

In the absence of pairing, the two species that we consider are the ur and dg quarks. In the presence of pairing, the ur particles ($\xi > 0$) and the dg holes ($\xi < 0$),

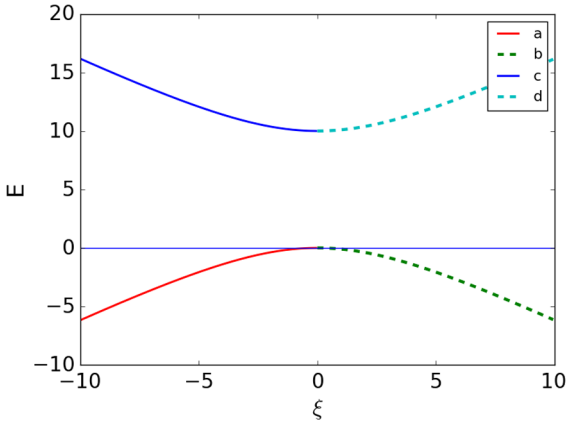

FIG. 1. The four [Eq. (26)] branches [solid red $(a, \xi < 0)$, dashed green $(b, \xi > 0)$, solid blue $(c, \xi < 0)$, and dashed cyan $(d, \xi > 0)$] for illustrative parameter values $\mu = 500$ MeV, $\Delta = 5$ MeV, $\delta\mu = 5.5$ MeV, $b = 5.2$ MeV, and $\cos\theta = -0.1$ [Eq. (25)]. The gap between the lower and upper branches is 2Δ, and for $\Delta \ll T$ only excitations near $E = 0$ participate in transport.

the ur holes and the dg particles mix with each other [86] [Eqs. (21) and (22)].

Therefore we take the four species as

$$\begin{aligned} a &\to E_1, \qquad \xi < 0, \\ b &\to E_1, \qquad \xi > 0, \\ c &\to E_2, \qquad \xi < 0, \\ d &\to E_2, \qquad \xi > 0. \end{aligned} \tag{26}$$

For an illustrative set of parameter values they are shown in Fig. 1. For $\xi \ll -\Delta$, the species a corresponds to ur particles and the species c for dg holes. Similarly, for $\xi \gg 0$ the species b corresponds to ur holes and the species d to dg particles. For $\xi \sim \Delta$, the mixing is substantial and the interpretation is not simple. In terms of the decomposition given in Eq. (C5), a corresponds to the modes γ for $\xi < 0$, b to γ for $\xi > 0$, c to the modes χ for $\xi < 0$, and d to χ for $\xi > 0$.

The matrix equation, Eq. (9), is now a 4×4 matrix equation which gives the four relaxation times τ_i and the viscosities can be found by using Eq. (18).

D. Interactions

The interactions between the quarks are mediated by the gluons and the photon. The gluon-quark vertex is

$$S_g = (g) \int d^4x \bar{\psi}\gamma^\mu t^m \psi A_\mu^m \tag{27}$$

where g is the strong coupling constant, and the photon-quark vertex is

$$S_e = (-e) \int d^4x \bar{\psi}\gamma^\mu Q \psi A_\mu \tag{28}$$

where t^m are the Gell-Mann matrices and $Q = \mathrm{diag}\{2/3, -1/3\}$ in flavor space.

Both the longitudinal and the transverse modes of $t^4 \cdots t^7$ in the FF phase are screened [87–89]. Therefore as discussed in Sec. II after Eq. (1) their contribution to scattering is subdominant compared to the Landau damped transverse mediators while calculating the transport properties. Hence we do not consider them further.

The fate of the t^8 and the photon Q is more interesting. As in the 2SC phase, the linear combination of t^8 and Q gives rise to the relevant gauge bosons like X and $\tilde{Q}$. The condensate turns out to be neutral under the linear combination associated with the $\tilde{Q}$ charge which is unscreened. The $\tilde{Q}$ photon is weakly coupled to the quarks and is less important than the unscreened gluons [31]. The orthogonal linear combination,

$$A_\mu^X = \cos\varphi A_\mu^8 + \sin\varphi A_\mu^Q, \tag{29}$$

with

$$\cos\varphi = \frac{\sqrt{3}g}{\sqrt{e^2 + 3g^2}}, \tag{30}$$

on the other hand is strongly coupled but still its contribution can be neglected as we argue later in this section.

The transverse t^1, t^2, t^3 gluons are not screened as in the 2SC phase [88,90]. It was shown in Ref. [61] that they are Landau damped. Therefore the most important mediator of interactions for the $ur - dg - ug - dr$ quarks is the t^1, t^2, and t^3 gluons as discussed in Sec. II.

The basic structure of the gluon propagator for the transverse t^1, t^2, t^3 gluons can be written from analogy with the transverse gluons in unpaired quark matter. The propagator for the transverse gluons in the absence of pairing has the structure

$$iD_{ij}^{ab} = \frac{i}{\omega^2 - \mathbf{q}^2 - \Pi_t(q)} [\delta_{ij} - \hat{q}_i\hat{q}_j]\delta^{ab} \tag{31}$$

where $(\omega, \mathbf{q}) = p_3^\mu - p_i^\mu = p_2^\mu - p_4^\mu$ is the four momentum carried by the gauge field, $\mathbf{q}^2 = \mathbf{q}\cdot\mathbf{q}$, $q = |\mathbf{q}|$, and where [29,56] Π_t is the transverse polarization tensor[3]

$$\Pi_t(\omega, q) \approx \left(\frac{-i\pi\omega}{4q}\right) 2N_f \left(\frac{g}{2}\right)^2 \frac{\mu^2}{\pi^2}. \tag{32}$$

In the unpaired phase (or any isotropic phase) the transverse projection operator is $[\delta_{ij} - \hat{q}_i\hat{q}_j]$ [see Eq. (31)]. This projects vectors in the subspace perpendicular to $\mathbf{q}$. In the

[3]The projection operator, also called Π in the previous section, always appears with indices $\Pi^{(n)}$ and can be easily distinguished from the polarization tensor.

absence of b, Π^{ij} is invariant under rotations about the $\mathbf{q}$ axis. But this is not true when b is present. Since there is a special direction $\hat{b}$, Π^{ij} can be projected further into components parallel and perpendicular to $\hat{b}$ which are also perpendicular to $\mathbf{q}$ [88]. The component parallel to $\hat{b}$ and perpendicular to $\mathbf{q}$ is called the "longitudinal transverse" whereas the component perpendicular to both $\hat{b}$ and $\mathbf{q}$ is the "transverse transverse" component. In the zero momentum limit the "longitudinal transverse gluon" has vanishing polarization tensor, whereas the "transverse transverse gluon" has a finite Meissner mass. The longitudinal transverse part of A_μ^X is long ranged as well as strongly coupled; its contribution is smaller compared to the t^1, t^2, t^3 gluons [below Eq. (38)].

To express the transverse polarization tensor in a compact form we choose an orthogonal basis as follows:

$$\hat{y}' = \frac{\hat{b}\times\hat{q}}{|\hat{b}\times\hat{q}|}$$
$$\hat{x}' = \hat{y}'\times\hat{q}. \tag{33}$$

Therefore, allowing the polarization tensor to depend on the direction we write the general form of the propagator for the exchange of the transverse t^1, t^2, t^3 gluons in the FF phase,

$$iD_{\mu\nu}^{ab} = \frac{i}{\omega^2 - q^2 - \Pi_t^{i'j'}(\omega,\mathbf{q})}[\mathcal{P}_{\mu\nu}^{i'j'}]\delta^{ab}. \tag{34}$$

Equation (34) is the generalization of Eq. (31) to systems with one preferred direction.

The projection operator,

$$\mathcal{P}_{\mu\nu}^{i'j'} = \delta_\mu^{i'}\delta_\nu^{j'}, \tag{35}$$

projects into the subspace spanned by the unit vectors e_i', e_j' [Eq. (33)].

The polarization functions $\Pi_t^{i'j'}(\omega,\mathbf{q})$ have a form,

$$\Pi_t^{i'j'}(\omega,\mathbf{q}) = \left(\frac{-i\pi\omega}{4q}\right)\left[2N_f(\frac{g}{2})^2\frac{\mu^2}{\pi^2}\right] \times h_t^{i'j'}\left(\frac{\Delta}{\delta\mu},\frac{b}{\delta\mu},\cos\theta_{bq}\right), \tag{36}$$

where h_t are dimensionless. For unpaired quark matter $h_t^{i'j'} = \delta^{i'j'}$.

Numerical results for the Landau damping coefficient for $b/\delta\mu = \zeta$ were found in Ref. [61] and are well described by the expressions

$$h_t^{x'x'}\left(\frac{\Delta}{\delta\mu},\frac{b}{\delta\mu},\cos\theta_{bq}\right) \approx 1 - \left(\frac{\Delta}{b}\right)^{1/4}\frac{1}{1.65}(1-\cos\theta_{bq}^4)^{1/2}$$
$$h_t^{y'y'}\left(\frac{\Delta}{\delta\mu},\frac{b}{\delta\mu},\cos\theta_{bq}\right) \approx 1 - \left(\frac{\Delta}{b}\right)\frac{1}{1.75}(1-\cos\theta_{bq}^2)^{1/2}$$
$$h_t^{x'y'}\left(\frac{\Delta}{\delta\mu},\frac{b}{\delta\mu},\cos\theta_{bq}\right) \approx 0. \tag{37}$$

We note that $h < 1$, which is expected because the gapless surface of the $ur - dg - ug - dr$ quarks in the FF phase has a smaller surface area compared to the unpaired phase. (For details see [39,72,74,75].)

The square of the scattering matrix element averaged over initial color and spin and summed over the final color and spin is given by[4]

$$\overline{|\mathcal{M}|^2}(ij_2\to j_3j_4) = 3\left(\frac{g}{2}\right)^4 |\mathbf{u}_{j_3}^\dagger\mathbf{u}_i|^2|\mathbf{u}_{j_4}^\dagger\mathbf{u}_{j_2}|^2 \frac{1}{4}\frac{1}{2p_i2p_22p_32p_4}\mathrm{tr}[\not{p}_3\gamma^\mu\not{p}_i\gamma^\nu]\mathrm{tr}[\not{p}_4\gamma^\sigma\not{p}_2\gamma^\lambda]D_{\mu\sigma}D_{\nu\lambda}$$
$$= 3\left(\frac{g}{2}\right)^4\delta_{ij_3}\delta_{j_2j_4}\frac{1}{4}\frac{1}{2p_i2p_22p_32p_4}\mathrm{tr}[\not{p}_3\gamma^\mu\not{p}_i\gamma^\nu]\mathrm{tr}[\not{p}_4\gamma^\sigma\not{p}_2\gamma^\lambda]D_{\mu\sigma}D_{\nu\lambda}, \tag{38}$$

where i, j_2, j_3, and j_4 run over 1,2 where 1 corresponds to γ and 2 to χ. Note that the orthogonality of $[\Phi]$ [Eq. (23)] ensures that $i = j_3$ and $j_2 = j_4$, and the nature of the Bogoliubov particles does not change at the vertex. This can be traced to the residual SU(2) symmetry in the two-flavor FF phase. The factor $1/(2p_i2p_22p_32p_4)$ appears in $\overline{|\mathcal{M}|^2}$ due to the convention of the phase space integrals in Eq. (11): the spinors u_s are normalized to be dimensionless.

The explicit form of the $\overline{|\mathcal{M}|^2}$ with the transverse interaction is given by

$$\overline{|\mathcal{M}|^2}(ij_2\to j_3j_4) = 3\left(\frac{g}{2}\right)^4\left(L_t^{xx}\frac{1}{|\mathbf{q}^2-w^2+\Pi_t^{xx}|^2} + L_t^{yy}\frac{1}{|\mathbf{q}^2-w^2+\Pi_t^{yy}|^2} + 2 \times \Re e\left[L_t^{xy}\frac{1}{\mathbf{q}^2-w^2+\Pi_t^{xx}}\frac{1}{\mathbf{q}^2-w^2+(\Pi_t^{yy})^*}\right]\right), \tag{39}$$

where

[4]The only subtle step is noting

$$\mathrm{tr}[\not{p}_3\gamma^0\gamma^\mu\gamma^0\not{p}_i\gamma^0\gamma^\nu\gamma^0] = \mathrm{tr}[\not{p}_3\gamma^\mu\not{p}_i\gamma^\nu]$$

if μ, ν are both spatial or both 0.

$$L_t^{xx} = (\cos(\phi_1)\cos(\phi_2))^2,$$
$$L_t^{yy} = (\sin(\phi_1)\sin(\phi_2))^2,$$
$$L_t^{xy} = \frac{1}{4}(\sin(2\phi_1)\sin(2\phi_2)),$$
$$L_t^{yx} = L_t^{xy}. \tag{40}$$

There are additional mediators of quark-quark interactions in the two-flavor FF phase. Phonons [91] associated with the periodicity of the condensate [50,92] are derivatively coupled to the fermion fields.

A rough estimate of the contribution to quark-quark scattering from phonon scattering can be obtained as follows. The interaction between quark species i and j, and phonon φ^a, can generically be written as

$$\mathcal{L}_{\varphi\psi} = \sum_{\nu=0}^{3} \frac{c_\nu}{f_\varphi^{ij}} \partial_\nu \varphi^a \bar{\psi}_j \gamma^\nu \psi_i, \tag{41}$$

where dimensionless couplings c_ν associated with the spatial derivatives of φ^a (c_0 corresponding to $\nu = 0$) and the temporal derivatives of φ^a ($c_\nu = c'$ for $\nu = 1, 2, 3$) are different in the finite density system. c_ν is naturally of the order of $v_F \sim 1$ in quark matter.

Therefore, the scattering matrix in the absence of pairing can be written as

$$i\mathcal{M} \sim \sum_{\nu\rho} \left(\frac{c_\rho q_\rho c_\nu q_\nu}{f_{\varphi^{ij}}^2}\right) \frac{i}{\omega^2 - v_\varphi^2 q^2} [\bar{u}_3 \gamma^\nu u_i][\bar{u}_4 \gamma^\rho u_2] \tag{42}$$

where $q_\rho = (\omega, \mathbf{q})_\rho$ is the four momentum carried by the phonon.

Using Eq. [62],

$$\omega \bar{u}(p+q)\gamma^0 u(p) - q^i \cdot \bar{u}(p+q)\gamma^i u(p) = 0, \tag{43}$$

and taking $\omega \ll \mathbf{q}$

$$i\mathcal{M} \sim \left(\frac{(c_0 + c')^2 \omega^2}{f_{\varphi^{ij}}^2}\right) \frac{-i}{v_\varphi^2 \mathbf{q}^2} [\bar{u}_3 \gamma^0 u_i][\bar{u}_4 \gamma^0 u_2]$$
$$\sim -i\left(\frac{(c_0 + c')^2}{f_{\varphi^{ij}}^2}\right) [\bar{u}_3 \gamma^0 u_i][\bar{u}_4 \gamma^0 u_2], \tag{44}$$

where we have used $\omega = c_\varphi |\mathbf{q}|$.

This should be compared with the matrix element for the exchange of a Debye screened gauge field,

$$i\mathcal{M} \sim (ig)^2 \frac{i}{q^2 + m_D^2} [\bar{u}_3 \gamma^0 u_i][\bar{u}_4 \gamma^0 u_2]$$
$$\sim -ig^2 \frac{1}{m_D^2} [\bar{u}_3 \gamma^0 u_i][\bar{u}_4 \gamma^0 u_2]. \tag{45}$$

Noting that both m_D and f_φ can be related to thermodynamic susceptibilities [64],

$$m_D^2 \sim g^2 f_\varphi^2, \tag{46}$$

we see that Eq. (44) is of the same order as Eq. (45) up to a factor of $(c + c')^2$ which is of the order of 1 in relativistic systems.[5] Therefore, the contributions to the quark-quark scatterings from phonon exchange are of the same order as the contribution from Debye screened gauge boson exchange. Since we have argued before that the Landau damped gauge bosons dominate over the Debye screened ones at low T and dropped the Debye screened gluon exchange contribution, we also drop the phonon mediated scatterings.

1. Simple model interaction

The form of the matrix element in Eq. (39) is quite complicated because of the anisotropy of Π_t in the FF phase. Therefore, to get some intuition we study the effect of the isotropic gapless pairing on the shear viscosity in Appendix E 1 for a simpler interaction of the form

$$\frac{g}{2} \bar{\psi} A_\mu \gamma^\mu \psi. \tag{47}$$

We also compute the shear viscosity in the FF phase for the same simple interaction [Eq. (47)] in Sec. IV A.

In the unpaired phase the longitudinal components of A_μ are Debye screened and we focus only on the longitudinal gluons so that we can zoom in to the effect of the change in the fermionic dispersion relations due to pairing. The relevant propagator for the gauge boson in the unpaired phase is

$$\frac{i}{\omega^2 - \mathbf{q}^2 - \Pi_l(q)} \tag{48}$$

where Π_l is the longitudinal polarization tensor. In the limit of small $\mathbf{q}$,

$$\Pi_l(q) \approx \Pi_l(0) = m_D^2 = 2N_f \left(\frac{g}{2}\right)^2 \frac{\mu^2}{\pi^2}, \tag{49}$$

up to corrections of the order $(\delta\mu/\mu)^2$.

The square of the matrix element averaged over initial spins and summed over the final spins [56] (after making some simplifying assumptions) is given by

$$\overline{|\mathcal{M}|^2}(ij_2 \to j_3 j_4) = \left(\frac{ig}{2}\right)^4 \times \left[\frac{1}{\mathbf{q}^2 + \Pi_l(0)}\right]^2 \left[1 - \frac{q^2}{4p_i p_3}\right] \left[1 - \frac{q^2}{4p_2 p_4}\right]. \tag{50}$$

The shear viscosity of unpaired quarks with this simple interaction is well studied [29,56]. The effect of pairing on

[5] In nonrelativistic systems [93], the magnetic gauge bosons do not contribute due to the small speeds and the exchange of phonons and the longitudinal gauge bosons compete. For $v_\varphi \ll 1$, the phonon exchange is the dominant scattering mechanism. We thank Sanjay Reddy for his comment on this point.

TABLE I. Quark and gluon spectra in the 2SC and in the FF phases.

	2SC	FF
Quark spectrum I	$ub - bd$, electrons unpaired	$ub - bd$, electrons unpaired
Quark spectrum II	$ur - dg - dr - ug$ gapped	$ur - dg - dr - ug$ gapless
t^1, t^2, t^3 (longitudinal)	Not Debye screened	Debye screened
t^1, t^2, t^3 (transverse)	Neither Meissner screened nor Landau damped	Landau damped
t^4, t^5, t^6, t^7	Debye and Meissner screened	Debye and Meissner screened
t^8, Q (longitudinal)	Debye screened	Debye screened
t^8, $Q \to X$ (transverse)	Meissner screened	One component Meissner screened One component Landau damped
t^8, $Q \to \tilde{Q}$ (transverse)	Landau damped	Landau damped

the shear viscosity for this interaction has not been studied, however, and we show how the contribution from the exchange of the longitudinal A_μ is affected by pairing in Appendix E 2.

In the paired phase the scattering matrix element for Bogoliubov quasiparticles [following the steps used for obtaining Eq. (38) for the longitudinal interaction of the form Eq. (47)] is given by

$$\begin{aligned}\overline{|\mathcal{M}|^2}(ij_2 \to j_3 j_4) &= \left(\frac{ig}{2}\right)^4 |[\Phi^*_{j_3 1}\Phi_{j_3 1} - \Phi^*_{j_1 2}\Phi_{i2}][\Phi^*_{j_4 1}\Phi_{j_4 1} - \Phi^*_{j_2 2}\Phi_{j_2 2}]|^2 \\ &\times \left[\frac{1}{\mathbf{q}^2 + \Pi_l(0)}\right]^2 \left[1 - \frac{q^2}{4p_i p_3}\right]\left[1 - \frac{q^2}{4p_2 p_4}\right] \qquad (51)\end{aligned}$$

where i's run over 1,2 corresponding to the two eigenstates given in Eq. (25). Φ's are the coherence factors [Eqs. (21) and (22)]. In the paired phase there are vertex corrections [94] for the longitudinal mode but since are only looking for qualitative insight for the simple interaction in this section, we do not consider these here.

We also use Eq. (47) in Sec. IV A to calculate the shear viscosity in the FF phase. This allows us to directly compare the results with unpaired quark matter and understand how the anisotropic dispersion relations change the shear viscosity, without the complication associated with the change in the gluon propagator [Eq. (36)].

All these help us to check our formalism for a simpler interaction and develop the intuition to understand our final result shown in Sec. IV B for the realistic magnetic interaction.

Finally, we remark that a comparison between Eqs. (38) and (51) can also be used to complete the argument that we made earlier about why the exchange of the transverse A^X_μ is less important than the exchange of t^1, t^2, t^3 even though they have zero Meissner mass. In matrix elements the exchange of the A^X_μ comes with a coherence factor [Eq. (51)] where two terms of similar size cancel. This is because $\Phi_{j_3 1}, \Phi_{j_3 1}, \Phi^*_{i2}$, and Φ_{i2} in Eq. (51) are all roughly $1/\sqrt{2}$ for $\xi \approx 0$ and in Eq. (51) their products appear with a $-$ sign. On the other hand the coherence factors in Eq. (38) add for the t^1, t^2, t^3 gluons. Therefore we expect the numerical contribution from A^X_μ to be smaller than the contribution from t^1, t^2, t^3 gluons. (There is an additional reduction by a factor of $\sim 1/2$ because the Transverse transverse gluon is massive.) Therefore we neglect the scatterings mediated by A^X_μ. This numerical suppression is not parametric and in a future, more complete calculation, these scatterings should be included. We note that A^X_μ induces coupling between the b quarks and the paired quarks and complicates the Boltzmann equation [Eq. (9)] significantly.

We summarize the quark and the gluon spectra of both the 2SC and the FF phase in Table I.

IV. RESULTS FOR ANISOTROPIC PAIRING

As discussed in the previous sections, pairing influences transport properties of fermions in two important ways. First, it modifies the dispersion relations of the fermions. Second, it changes the mediator interactions. We discuss how salient features of transport properties in the FF phase emerge because of intricate interplay of these factors.

To get some understanding of how the modification of the dispersion relations due to pairing affects transport, we solve the Boltzmann equations for simple model interactions of quark mediated by the Debye screened longitudinal gluons in the next section. In the section after that we show the analysis for the two-flavor FF phase with the realistic interaction: exchange of the transverse t^1, t^2, and t^3 gauge bosons. That section contains the main results of the paper.

To evaluate the integrals in the lhs (L_i) and the rhs (R_{ij}) appearing in the Boltzmann equation [Eqs. (10) and (11)] with the dispersions [Eq. (25)] for any given T and $\delta\mu$, we need Δ and b as a function of $\delta\mu$. For a given b and $\delta\mu$, Δ can be found by solving the gap equation for the FF phase [75]. b is fixed by Eq. (5).

We take the solution of the gap equation, Δ, as a function of $\delta\mu$, from the topmost curve (green online) in Fig. 3 in Ref. [75]. The calculations in Ref. [75] were performed for a three-flavor FF phase which is very similar to the

two-flavor FF phase, and we use these results here. (See Fig. 2 and the discussion below in Ref. [75].)

As mentioned earlier in Sec. II, to explore the parameter space in $\delta\mu$ where FF or LOFF like phases might be the ground state, we vary $\delta\mu/\Delta_0 \in (0.575, 0.75)$.

A. Debye screened gluon exchange

We first perform the analysis of the shear viscosity of the FF phase for a simple model of quark interaction, Eq. (47) for the two species ψ_1, ψ_2 where $\psi = (\psi_1, \psi_2)^T$ in Eq. (47). The form of the matrix element is given in Eq. (51).

First we specify the relevant variables. We note that we can set the overall scale in terms of the chemical potential μ. Then the quantities, L_i/μ^4, R_{ij}/μ^5, $\tau\mu$, and η/μ^3, are dimensionless and can be written as functions of the variables $(\frac{T}{\mu}, \frac{\delta\mu}{\mu}, \frac{b}{\mu}, \frac{\Delta}{\mu})$. The quantities b/μ and Δ/μ are fixed by using the solution of the gap equation in a FF phase as discussed above. Therefore, one needs to only explore how the viscosity changes as we change T/μ and $\delta\mu/\mu$. In Figs. 2 and 3 we fix the value of $T/\mu = 3.34 \times 10^{-4}$, and explore how the viscosity varies with the dimensionless ratio $\delta\mu/\Delta_0$ in the range $\delta\mu/\Delta_0 \in (0.575, 0.75)$.

For a fixed μ, there are two dimensionless ratios that are needed to specify the transport properties of the FF phase as a function of $\delta\mu$ and they are T/μ and Δ_0/μ. We show the results for $T/\mu = 3.34 \times 10^{-4}$ and $\Delta_0/\mu = 1.67 \times 10^{-2}$ in Figs. 2 and 3. To get a concrete feel for numbers, one can take $\mu = 600$ MeV, $\Delta_0 = 10$ MeV and $T = 0.2$ MeV.

In the top panel of Fig. 2 we plot the results for L_i as a function of $\delta\mu$. To calculate L_i we have used Eq. (10) and the anisotropic dispersion relation in Eq. (25). The results for a and b species are shown by the upper solid curve interpolating the filled circles (red online). The error in the numerical evaluation of L_i is negligible. For comparison, Eq. (52) is shown by the upper dot dashed line (yellow online) in the top panel of Fig. 2.

In the lower panel of Fig. 2 we plot the results for R_{ij} as a function of $\delta\mu$ evaluated using Eq. (11) with Eqs. (B7), (B11) and (B12). For comparison, Eq. (54) is shown by the upper dot dashed line (yellow online) on the top right panel of Fig. 2.

Unpaired quark matter, discussed in Appendix E 1 for the same interaction, provides a benchmark to compare the quantities L_i/μ^4, R_{ij}/μ^5, $\tau_i\mu$, and η_i/μ^3. We show the numerically obtained results for L_i [Eq. (E1)] and R_{ij} [Eq. (E3)] in Fig. 2, and η_i [$\eta_i = -3\nu_1(L_1^{\rm un})^2/4s_1^{\rm un}$ where $\nu_1 = 2$ and $s_1^{\rm un}$ is given in Eqs. (E3)] for unpaired quark matter in Fig. 3. They are denoted by dashed curves (black online).

The curves for L_i and R_{ii} in Fig. 2 for the FF phase and for unpaired matter individually change if T/μ is changed. In particular, the dependence of L_i (R_{ii}) on T/μ for unpaired quarks is given in Eq. (E2) [Eq. (E5)]. Similarly, in Fig. 3, η for the FF phase and for unpaired quarks will change on changing T/μ. The dependence of η for unpaired quarks on T/μ is given in Eq. (E6).

However the ratio of the transport properties in the FF phase to unpaired quarks for a fixed $\delta\mu/\mu$ does not change as we change T/μ. Hence it is useful to summarize the dependence of η for the FF phase on both T/μ and $\delta\mu/\mu$ by quoting the ratio of L_i, R_{ij}, and η in the FF phase to the result for unpaired quarks, as is shown in Eqs. (52), (54), and (57) respectively. This feature is shown in more explicit detail in Sec. IV B where the dependence of the viscosity on both $\delta\mu/\mu$ and T/μ is separately plotted for the interactions mediated by transverse gluon exchange.

The key point in understanding the results for the FF phase is that the branches a and b are gapless for $\cos\theta \in [\frac{-\delta\mu+\Delta}{b}, 1]$ throughout the range $\delta\mu/\Delta_0 \in (0.575, 0.75)$ while the branches c and d are gapped. A simpler phase with the same feature is the isotropic gapless phase. Therefore the reader might find it useful to understand the results for

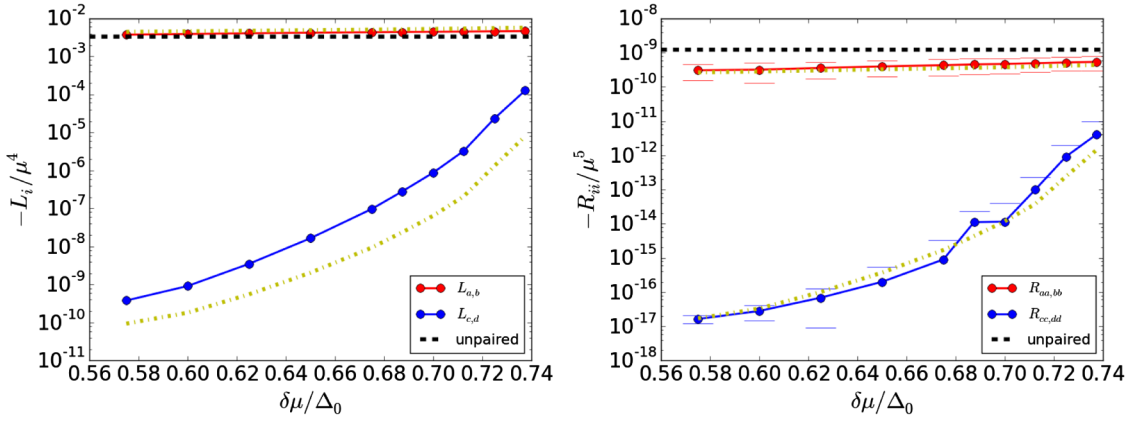

FIG. 2. Plots of L_i (upper panel) and the diagonal entries of R_{ij} (lower panel) for $T/\mu = 3.34 \times 10^{-4}$ and $\Delta_0/\mu = 1.67 \times 10^{-2}$ fixed for the interaction given in Eq. (51). The upper dot dashed curves (yellow online) in the panels for L_a and L_b (R_{aa}, R_{bb}) correspond to Eq. (52) [Eq. (54)]. The lower dot dashed curves in the panels for L_c and L_d (R_{cc}, R_{dd}) correspond to Eq. (53) [Eq. (55)].

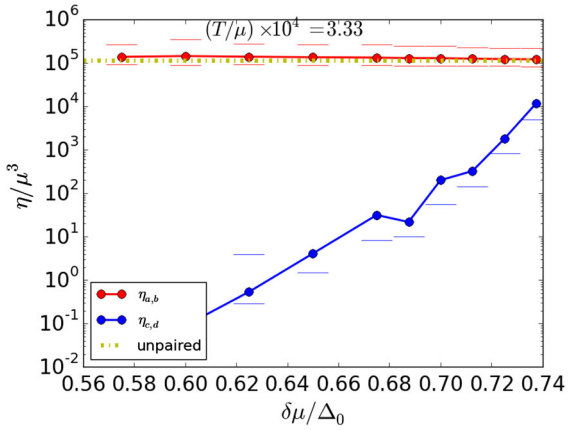

FIG. 3. Plot of η_i from L_i and R_{ij} shown in Fig. 2. The dot dashed line (yellow online) corresponds to η_1^{un}.

the isotropic gapless phase described in detail in Appendix 2 b and summarized in Eqs. (E24) and (E25) and Fig. 10.

The phase space for the gapless dispersion branches a and b receives correction in contrast to the isotropic gapless phase [Eq. (E22)] due to the fact that the gapless surface is the boundary of a crescent with arc length $1+\frac{\delta\mu-\Delta}{b}$ instead of 2. Therefore, we expect that L_i has a geometric reduction in comparison to the unpaired quark matter as follows

$$L_a = L_b = L^{\rm un} \times \mathrm{f}_1\left(\frac{\delta\mu}{b},\frac{\Delta}{b}\right) \approx L^{\rm un} \times \frac{1}{2}\left(1+\frac{\delta\mu}{b}-\frac{\Delta}{b}\right) \tag{52}$$

where f_1 is a dimensionless function smaller than 1 corresponding to the limited range of angles for which the modes are gapless.

The branches c and d are gapped for $\delta\mu/\Delta_0 < 0.735$ and hence L_c and L_d are exponentially suppressed. A rough estimate is $L_c = L_d \sim e^{-\Delta/T}$. The lower dot dashed curve (yellow online) corresponds to

$$L_{c,d} \sim L^{\rm un} e^{-\Delta/T} \tag{53}$$

and captures the behavior of the numerical result [lower solid curve (blue online) in the top panel of Fig. 2] up to a scale factor. The proportionality factor depends upon T. Since the contribution of species c, d to transport is suppressed exponentially, we do not explore this further.

Similarly, R_{ij} is expected to be suppressed by the square of the phase space factor,

$$R_{aa} = R_{bb} \approx \frac{1}{2}R_{11}^{\rm un} \times \left(\frac{1}{2}\left(1+\frac{\delta\mu}{b}-\frac{\Delta}{b}\right)\right)^2. \tag{54}$$

R_{cc} and R_{dd} are exponentially suppressed and their numerical evaluation is noisy (see Appendix F for details). A rough estimate that we found roughly matches the numerical results for these components is

$$R_{cc} = R_{dd} \approx R_{11}^{\rm un} \times e^{-\Delta/T}. \tag{55}$$

τ and η can be obtained using Eqs. (9) and (18) and the results for η are shown in Fig. 3. From Eqs. (52) and (54) we expect

$$\tau_a = \tau_b \approx 2\tau_1^{\rm un}, \tag{56}$$

and

$$\eta_a = \eta_b \approx \eta_1^{\rm un} \tag{57}$$

[the form of $\eta_1^{\rm un}$ is given in Eq. (E6)]. On the other hand,

$$\eta_c = \eta_d \sim \eta_1^{\rm un} e^{-\Delta/T}. \tag{58}$$

Consequently,

$$\eta(b\neq 0) = \sum_i \eta_i \approx \eta_a + \eta_b \approx 2\eta_1^{\rm un}. \tag{59}$$

The 16 components of R_{ij} are evaluated separately using Monte Carlo integration [Eq. (B7)]. To improve the statistics, we have averaged R_{aa} and R_{bb} (which should be equal), and R_{ab} and R_{ba} (which should be equal) while making Fig. 2 and adding the errors in quadrature. Similarly, we have combined the data for the c and d branches in Fig. 5. The central values of R_{ij} are given by filled circles and the error bars (from the Monte Carlo integration for R_{ij}) are shown by the dashes of the same color and propagated to errors in η (Fig. 3). The numerical results roughly match analytic expectations [Eqs. (54) and (55)].

The numerical results for η are shown in Fig. 3 and agree well with Eq. (59). The upper branch (circles with error bars) corresponds to $\eta_{a,b}$ and the lower to $\eta_{c,d}$. Note that some points in the lower branch do not show an upper error bar. These correspond to parameters where the result for $\eta_{c,d}$ with the upper estimate of $R_{cc,dd}$ is negative and therefore these values of η do not show up on the log plot. This is a consequence of the fact that the numerical errors in the small components $R_{cc,dd}$ can be comparable or larger than the values of R_{ij} itself, though this is not important here because c, d contribute only minimally to the shear viscosity. This issue is exacerbated in Sec. IV B where even the larger components of R_{ij} are difficult to compute accurately for all parameter values.

Equation (59) is a remarkable result and is a consequence of the intricate interplay between τ and η. The reduced phase space due to pairing increases τ_a and τ_b ($\tau \propto L.H.S/R.H.S$), whereas, in the product $\eta \propto L.H.S\tau$, the two effects cancel out and η remains the same.

The key results that we obtained in this section are mentioned below. For the interaction given in Eq. (51),

(1) L_a and L_b are only geometrically suppressed by the smaller gapless surface [Eq. (52)].

(2) L_c and L_d are exponentially suppressed compared to L_a, L_b.
(3) For Debye screened mediators, R_{aa} and R_{bb} are only geometrically suppressed [Eq. (54)].
(4) R_{cc} and R_{dd} are exponentially suppressed.
(5) $\eta \approx \eta^{\rm un}$.

B. t^1, t^2, t^3 gluon exchange

Now we use the interaction mediated by the Landau damped t^1, t^2, t^3 to calculate η in the two-flavor FF phase. In this section we show the results for the $ur - dg$ sector with Bogoliubov quasiparticles given by Eqs. (21) and (22). The $ug - dr$ sector gives an identical contribution.

In Eq. (10), L_i depends only on the spectrum of quasiparticles and not the interaction; hence, they are not modified and can be read off from Eq. (52).

The difference from the previous section appears in the collision integral $[R_{ij}]$ (compare Figs. 2 and 4), where the square of the matrix element $\overline{|\mathcal{M}|^2}$ is given by Eq. (39) (Fig. 4) instead of Eq. (51) (Fig. 2). The values of T/μ and Δ_0/μ are chosen to be the same as in the previous section (caption of Fig. 2).

The first difference to note between the lower panel of Figs. 2 and 4 is the difference in the overall scale [29,56]. The reference horizontal line for the unpaired quarks in Fig. 4 is roughly a factor $(\frac{3}{2^{1/6}})(\frac{g\mu}{\pi^2 T})^{1/3}$ larger than the corresponding line in Fig. 2 as explained in Eq. (E8) in Appendix E 1 a.

The nontrivial result for R_{aa} and R_{bb} in the FF phase is that they are *enhanced over* the unpaired isotropic result, unlike what was observed in Fig. 2 for Eq. (51). The intuitive explanation for this is as follows.

There are two competing phenomena which determine the nature of the collision integral. As seen in Sec. IV A, the geometric suppression due to the smaller gapless surface [Eq. (54)] leads to a reduction in R_{aa} and R_{bb}.

For $\mathbf{q} \ll \mu$ the collision kernel receives enhancement from the Jacobian for the transformation from the energy δ functions to the momentum δ functions. In more detail, from Eq. (B7) it is seen that after solving the two delta functions simultaneously Jacobian (J_q) arises in the denominator, which is proportional to $J_q \propto v_{p_i,p_2} \propto \xi_{\mathbf{p}_{i,2}}/\sqrt{\xi^2_{\mathbf{p}_{i,2}} + \Delta^2}$. For $|\delta\mu + b\cos\theta| \approx \Delta$, the dispersion is gapless for $\xi \approx 0$ [Eq. (A5)], which implies $v_{p_{1,2}} \to 0$ and the Jacobian for the δ functions diverges. [The detailed form of the Jacobian is described near Eq. (B13) in Appendix B.] Higher order terms in the Taylor expansion of ξ_p prevent R_{ij} from diverging, but this shows up as an increase in R_{ij}. A similar phenomenon for the isotropic gapless CFL phase was seen earlier in Ref. [95]. Hence, the reduced phase space tries to lower the value of the rhs whereas the denominator tries to compensate the effect. Effectively one obtains enhanced R_{ij} compared to unpaired quark matter.

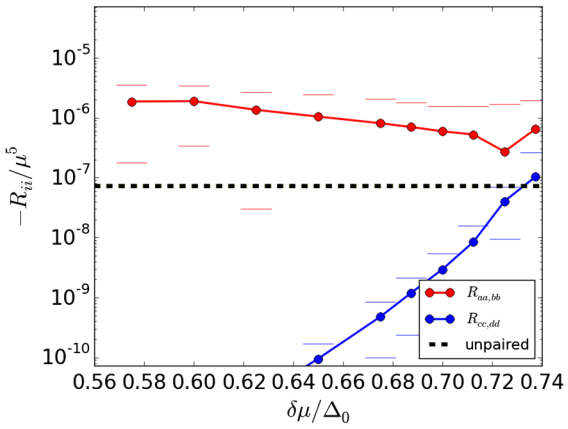

FIG. 4. Plots of the diagonal entries of R_{ij} for $T/\mu = 3.34 \times 10^{-4}$ and $\Delta_0/\mu = 1.67 \times 10^{-2}$ fixed for the matrix element given in Eq. (38). The dashed horizontal line (black online) corresponds to $R^{\rm run}$ [Eq. (E8)].

There are two reasons why this effect is not seen in Fig. 3 where the interaction is mediated by the Debye screened gluons. First, the relative $-$ sign between the coherence factors in Eq. (51) compared with the $+$ sign in Eq. (38) implies that the matrix element given in Eq. (51) tends to 0 if $\xi \to 0$ while Eq. (38) does not. Second, one can see from the structure of the propagator, if $q \sim g\mu$ then only the screening effect becomes important. On the other hand for the transverse sector, since $\omega \sim T \ll g\mu$ and $q \sim g\mu$ the collision integral is dominated by small $\mathbf{q}$ compared to μ. Hence, one can conclude that the enhancement effect is more pronounced where the exchanged gauge boson is Landau damped.[6]

We make one technical comment about the numerical evaluation of R_{ij} in Fig. 4. Because of the more sharply peaked nature of the integrand due to the two reasons mentioned above, the Monte Carlo integration for R_{ij} [Eq. (B7)] converges more slowly. Even with a factor of 5 larger number of sampling points compared to Fig. 2 (see Appendix F for details on the numerical implementation), the value corresponding to the lower error bar for the upper branch $-R_{aa,bb}$ is negative and does not show up in the log plot for multiple values of $\delta\mu$. In the results for η it shows up as missing upper error bars. The relative errors are larger for lower T.

The results for η for four different values of the temperatures are shown in Fig. 5. In all four cases it shows a reduction in η by a factor of roughly 100 compared to unpaired quark matter, associated with the enhancement in the collision integral.

[6]There is an additional source of enhancement when the gauge boson polarization is given by Eq. (32) or Eq. (36) rather than Eq. (49). Since $h < 1$, $\overline{|\mathcal{M}|^2}$ is larger in the anisotropic paired phase than the isotropic unpaired phase. However, since h is not $\ll 1$ for all $\cos\theta$, this is not the dominant effect.

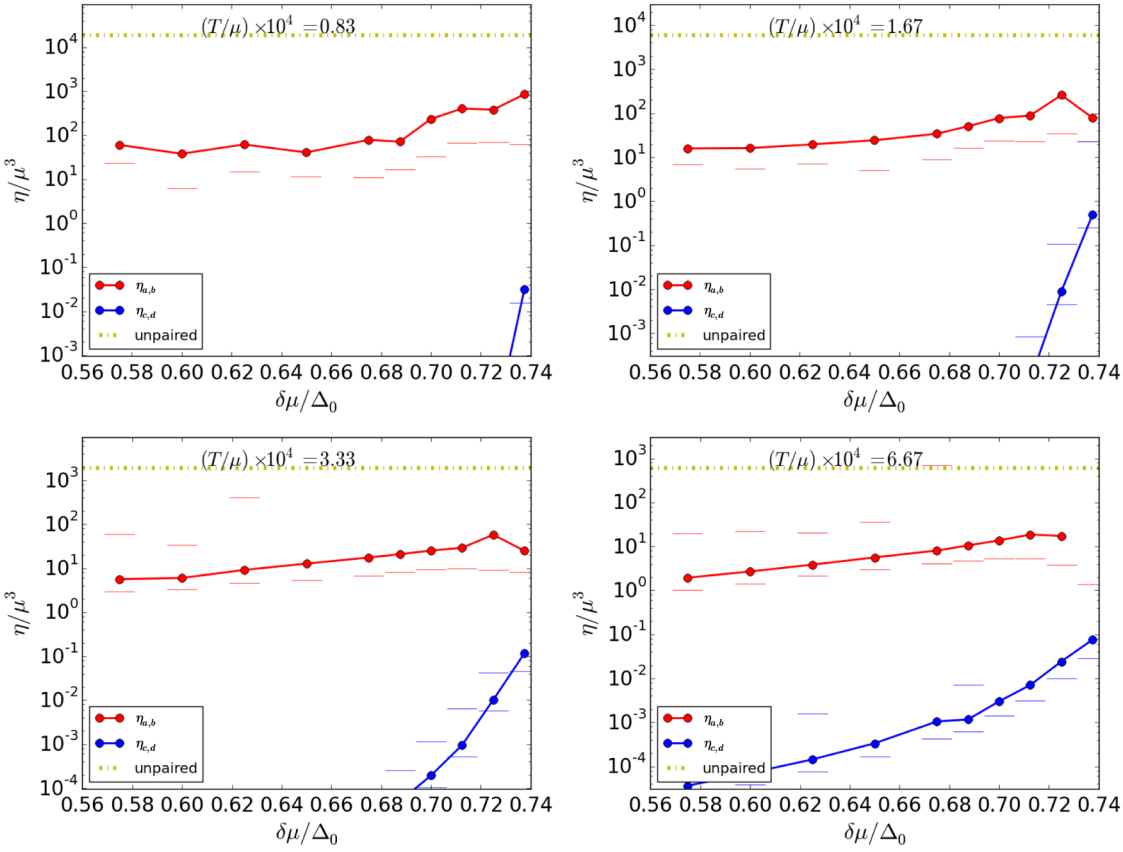

FIG. 5. Plots of η_i with $b \neq 0$ [for matrix element Eq. (38)] for four different values of T/μ with $\Delta_0/\mu = 1.67 \times 10^{-2}$ fixed. The dot-dashed curve (yellow online) shows $\eta_1^{\rm tun}$.

Figure 6 shows viscosity as a function of T/μ for the $ur - dg$ quarks in the FF phase for a fixed $\delta\mu/\mu = 10^{-2}$.

The result for the FF phase is denoted by the solid points with errors denoted by error bars. The error bars are large enough that we do not attempt a fit but a rough description of the central points of the data in this T range is given by

$$\eta \sim 10^{-2}\eta_1^{\rm tun}. \tag{60}$$

Since η is relatively flat with respect to $\delta\mu$ for all the T's in a wide range of $T \ll \Delta$ (Fig. 4), we propose Eq. (60) as a fair parametrization of the shear viscosity in the FF phase for $T \ll \Delta$ throughout the two-flavor FF window. Equation (60) is a concise summary of our main result.

For comparison we have shown the electron contribution [shown as a dark dot-dashed curve (blue online)] and the bd contribution [shown as a dark dashed curve (blue online)] in Fig. (60). These were calculated using the approximate analytic expressions given in Eqs. (78)–(80) in Ref. [56]. Note that these are even larger than the results for unpaired quark matter [shown as a light dot-dashed curve (yellow online)] because for the bd quarks the exchanged gluons t^8 and t^X are screened rather than Landau damped, while the e's couple weakly. Therefore these two modes dominate the viscosity in the two-flavor FF phase.

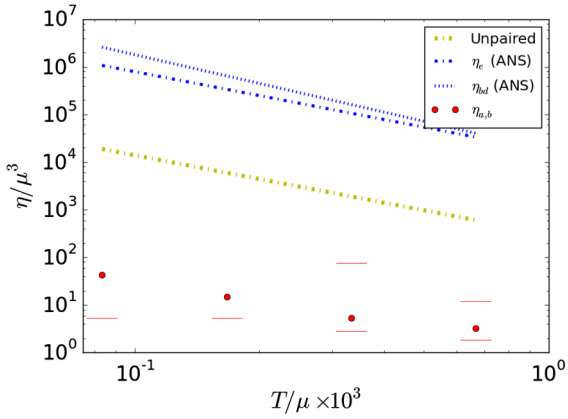

FIG. 6. η_i for species a and b for anisotropic pairing with $\Delta/\Delta_0 = 0.35$, $\delta\mu/\Delta_0 = 0.6$, and $\mathbf{b} = 1.2\delta\mu$ as a function of T. The viscosity for the FF phase is shown by solid red points obtained from the four panels of Fig. 5. The electron contribution [shown as a dark dot-dashed curve (blue online)] and the bd contribution [shown as a dark dashed curve (blue online)] are calculated using expressions given in Ref. [56] by M. G. Alford, H. Nishimura, and A. Sedrakian (ANS).

V. CONCLUSIONS

We present the first calculation of the shear viscosity of the two-flavor FF phase of quark matter.

We identify the low energy quasiparticles that play an important role in transporting momentum and energy at low T. Due to the large density of states near the Fermi surface, the u and d quarks, and the electrons dominate transport properties if they are gapless. The blue u and d quarks, and the electrons do not participate in pairing and their viscosity is the same as in the 2SC phase, calculated in Ref. [56].

The $ur - dg - ug - dr$ quarks pair and form Bogoliubov quasiparticles. The main difference between the two-flavor FF and the 2SC phase is that the spectra of Bogoliubov quasiparticles feature gapless modes near the boundaries of the crescent-shaped blocking regions. The technical advance made in the paper is the calculation of their viscosity.

The other low energy modes, the phonons associated with the compressions and rarefactions of the isophase surfaces of the order parameter [50], are Landau damped and do not contribute significantly to the energy-momentum transport at low temperatures.

By comparing the strength and the ranges of the particles that mediate quark interactions (see Sec. III D for details) we conclude that the dominant mechanism of scattering of the $ur - dg - ug - dr$ Bogoliubov quasiparticles in the two-flavor FF phase is the exchange of the transverse t^1, t^2 and t^3 gluons which are Landau damped. Note, in particular, that the longitudinal t^1, t^2 and t^3 gluons are Debye screened and therefore their contribution to quark-quark scattering can be ignored compared to the transverse t^1, t^2 and t^3 gluons. The Landau damping is anisotropic. Details about the gluon polarization tensor are given in Ref. [61]. We also show that the scattering of the Bogoliubov quasiparticles via exchange of the Goldstone modes, and due to their absorption and emission, is subdominant for $T \ll \mu$ and can be ignored.

We give a novel formalism to describe the scattering of Bogoliubov quasiparticles. We separate the two branches of the quasiparticle dispersions into $\xi > 0$ and $\xi < 0$ modes. This doubles the dimension of the collision integral matrix, with four modes a, b, c and d. The utility of this formalism is that it interpolates between two pairing regimes. When T is comparable to Δ (near the superconducting phase transition) the collision integral includes processes involving $a + c \to a + c$ ("interband" processes). When $T \ll \Delta$ the collision integral only features $a + a \to a + a$, $b + b \to b + b$, and $a + b \to a + b$ ("intraband" processes). Pair breaking processes are frozen. For isotropic gapless pairing in this regime ($b = 0$, $\delta\mu > \Delta$) a simpler formalism involving only the E_1 branch would be sufficient. The subtlety in the FF phases is that both the E_1 and the E_2 branches can become gapless depending on the values of b, $\delta\mu$, Δ and the angle θ of the momentum with the $\hat{b}$ direction. Our formalism allows for all these possibilities.

Our main result is given in Figs. 5 and 6. The key result is that the viscosity of the $ur - dg - ug - dr$ quarks for a wide range of $\delta\mu$ in the LOFF window is reduced by a factor of roughly 10^{-2} compared to the viscosity of unpaired quarks interacting via the Landau damped transverse gluons. This is summarized in a compact parametrization of the viscosity in Eq. (60).

This is a surprising result. In the 2SC phase the $ur - dg - ug - dr$ quarks are fully gapped and are frozen. In the FF phase the geometric area of the gapless surface is reduced by pairing. But at the same time the phase space for collisions is also reduced by the square of the geometric factor. Hence this simple argument suggests that the shear viscosity should be comparable to that for the unpaired quarks. Indeed this is precisely what happens if the interaction between the quarks is assumed to be mediated by the Debye screened longitudinal gluons corresponding to the broken generators, as shown in Fig. 3. For long-range interactions (dominated by smaller momentum exchanges), however, there is an additional effect due to the increase of the density of states satisfying the energy conservation equation due to small velocities over a part of the Fermi surface. The collision integral is enhanced and the shear viscosity is reduced [Eq. (60)]. This effect is particularly pronounced for t^1, t^2, t^3 gluons because the coherence factors in the matrix element do not cancel [Eq. (38)].

Comparing the shear viscosity of the gapless quarks in the FF phase with the contributions of the unpaired ub and db quarks and the electrons for the 2SC phase in Ref. [56] which remain comparable in the anisotropic phase also, one can argue that the unpaired quarks and the electrons give the shear viscosity of the two-flavor FF phase to a very good approximation.

In this paper we have only given results for the projection operator $\Pi^{(0)}$. It will be interesting to repeat the calculation for the other projection operators $\Pi^{(1)}$ and $\Pi^{(2)}$ ($\Pi^{(3)}$ and $\Pi^{(4)}$ are Hall projections and the associated viscosities are expected to be 0 in a system without magnetic fields). The difference between the three projection operators like Π_0, Π_1 and Π_2 is related to the anisotropic viscosity tensor and might have interesting implications. Although, the condensation in multiple directions will tend to isotropic the shear viscosity.

Looking ahead, one can think of several advances that can improve our calculation, for example, considering more complicated pairing patterns and including the strange quarks. In the following discussion we attempt to present a plausible picture of how the shear viscosity of these more realistic phases might behave based on the intuition gained from our calculation, and make some speculations about the physical implications for neutron star phenomenology.

For example, one can consider more realistic two-flavor LOFF structures [74] involving multiple plane waves. The details of these more complex condensates [91] featuring gapless fermionic excitations, remain complicated. The two main features, (a) gapless quasiparticle excitations over a Fermi surface with a complicated shape and (b) the Landau damping of transverse t^1, t^2, and t^3 gluons are expected to be present also in these more complicated phases.

Consequently the shear viscosity of the $ur - dg - ug - dr$ quarks can be ignored as in the FF phase.

Depending on the strange quark mass and the coupling strength between quarks, quark matter in neutron stars may also feature strange quarks. In the 2SC + s phase, the electron number is suppressed and numerous unpaired strange quarks contribute to transport. One expects their contributions to be comparable to that of the ub and db quarks in the 2SC phase. The same is also expected for the two FF + s phase.[7] In all these cases our calculation suggests that whether unpaired s quarks are present or not it is impossible to distinguish two-flavor LOFF pairing from 2SC pairing by comparing the shear viscosity of the two phases. The paired quarks are suppressed, though not exponentially.

Qualitative differences, however, are expected to arise if the strange quarks are also paired. That is, the three-flavor FF [75] or three-flavor LOFF phases [41]. In these phases the electrons are few in number and can be ignored as a first approximation. The fermionic excitations are gapless on nontrivial surfaces [75], as in the two-flavor case. It would be compelling to formulate the theory in the three-flavor FF phase. The result could have implications on the observed distribution of the neutron stars in the temperature vs rotational frequency (Ω) plot [6].

Currently, the temperatures of several fast spinning neutron stars are not well known (they are simply upper bounds), and no neutron stars are known which lie close to the shear viscosity stability edge (cooler than 10^7 K). A discovery of such a star could, in principle, distinguish between the three-flavor paired and unpaired quark matter as the source of damping of r-modes, if one can simultaneously pin down the damping by other mechanisms (for example, phase boundaries or Eckman layers).

Making this speculation more quantitative requires a better estimate of the LOFF window in the three-flavor quark matter, making models of hybrid neutron stars with quark matter and LOFF cores with equations of states compatible with recent constraints on masses and radii of neutron stars, and a calculation of the shear viscosity in three-flavor LOFF phases as a function of the T and μ.

Presently, stronger constraints on the viscosities of dense matter come from hotter, fast rotating neutron stars. The bulk viscosity provides the damping mechanism in this regime and only selected phases of dense matter are consistent with the observations unless r-modes saturate at small amplitudes [6]. Since the bulk viscosity in quark matter does not involve the scattering between two quarks it is not sensitive to the nature of screening of the gluons but it is sensitive to the presence of the gapless quark modes. Therefore it may be interesting to calculate the bulk viscosity in these phases to find out how the geometric reduction in the gapless surface affects the bulk viscosity in LOFF phases.

[7]Some details will be modified. The t^1, t^2 and t^3 will get additional Landau damping contributions from the s quarks. The qualitative answers, however, are not expected to change.

ACKNOWLEDGMENTS

We thank the workshop on the Phases of Dense Matter organized at the Institute For Nuclear Theory (INT) at the University of Washington, Seattle, where part of this work was completed. We thank Mark Alford, Nils Andersson, Sophia Han, Sanjay Reddy, Andras Schmitt and especially Kai Schwenzer for discussions. Sreemoyee Sarkar acknowledges the support of Department of Science and Technology (DST) under the INSPIRE faculty award. We also thank Prashanth Jaikumar for his comments.

APPENDIX A: PAIRING AND BLOCKING REGIONS

Evaluation of the shear viscosity requires figuring out the relevant FF phase space in which multispecies scatterings occur. It is necessary to have an idea of the FF phase space since this explains which fermionic modes are gapless and are relevant for transport. Here we describe the salient aspects of the FF phase space. For details please see [39,72].

At $T = 0$ (and almost so for $T \ll \Delta, \delta\mu$), all energy eigenstates with $E < 0$ are filled and the $E > 0$ eigenstates are empty. This defines the pairing and the blocking regions. In Fig. 7 the dotted circle depicts the $\xi = 0$ curve, i.e., along the circle $p = \mu$. The upper crescent-shaped region corresponds to the blocking region for d quarks and the lower shaded region is the blocking region for u quarks. These regions are where only one species of quarks is present and therefore are not conducive to pairing. In the presence of finite interactions, i.e. nonzero value of the gap parameter, the upper and lower blocking regions are separated by a small

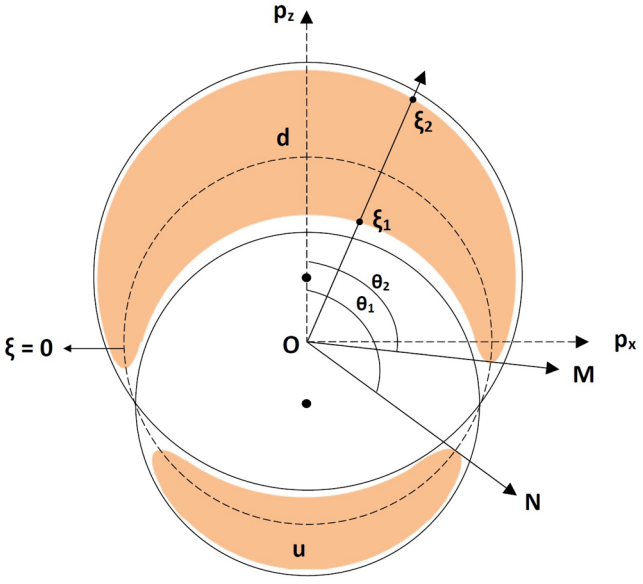

FIG. 7. Pairing and blocking regions of the LOFF phase space.

window. The complementary region is the pairing region. The pairing as well as the blocking regions are restricted by certain values of ξ and θ which we describe below.

In the pairing region $E_1 < 0$ and $E_2 > 0$ [Eq. (25)] and the quasiparticle excitation energies (the magnitude of the dispersion relations) are given by

$$E_-(\xi,\theta) = E_1 = -\delta\mu - b\cos\theta + \sqrt{\xi^2+\Delta^2},$$
$$E_+(\xi,\theta) = E_2 = \delta\mu + b\cos\theta + \sqrt{\xi^2+\Delta^2}. \quad \text{(A1)}$$

The interplay of limits of $\cos\theta$ and ξ determines the boundaries of pairing and blocking regions. From Fig. 7 it is evident that the regime that falls in between $\cos\theta \in [-1, \cos\theta_1]$ and ξ bounded by ξ_1 and ξ_2 i.e.$\xi \in [-\infty, \xi_1] \cup [\xi_2, \infty]$ is the lower pairing region. The region which is bounded by the limits $\cos\theta \in [\cos\theta_2, 1]$ and $\xi \in [-\infty, \xi_1] \cup [\xi_2, \infty]$ is the upper pairing region. The regime lying in between these two crescent-shaped zones has the bounds $\cos\theta \in [\cos\theta_1, \cos\theta_2]$ and $\xi \in [-\infty, \infty]$. The values of θ_1 and θ_2 can be obtained by solving the dispersion relations as mentioned in Eq. (A1) with the condition $\xi = 0$. This is required since at the edges dispersion relations are gapless which depict both $E_{1,2} = 0$ and $\xi = 0$. The limits of ξ can be obtained by putting the conditions $E_{1,2} = 0$. These conditions can be expressed in a concise way as follows.

(i) The lower pairing region,

$$\cos\theta \in \left[-1, \max\left(\frac{-\delta\mu-\Delta}{b}, -1\right)\right],$$
$$\xi \in \left(-\infty, -\sqrt{(\delta\mu + b\cos\theta)^2 - \Delta^2}\right)$$
$$\cup \left(\sqrt{(\delta\mu + b\cos\theta)^2 - \Delta^2}, \infty\right). \quad \text{(A2)}$$

(ii) The regime of small window,

$$\cos\theta \in \left[\frac{-\delta\mu-\Delta}{b}\frac{-\delta\mu+\Delta}{b}\right],$$
$$\xi \in (-\infty, +\infty). \quad \text{(A3)}$$

(iii) The upper pairing region,

$$\cos\theta \in \left[\min\left(\frac{-\delta\mu+\Delta}{b}, 1\right), 1\right],$$
$$\xi \in \left(-\infty, -\sqrt{(\delta\mu + b\cos\theta)^2 - \Delta^2}\right)$$
$$\cup \left(\sqrt{(\delta\mu + b\cos\theta)^2 - \Delta^2}, \infty\right). \quad \text{(A4)}$$

The system is cylindrically symmetric and the polar angle $\phi \in [0, 2\pi]$. From Eq. (A3) it is clear that the angular width between the two crescent-shaped regions is $2\Delta/b$. The complementary region in momentum space is the blocking region consisting of two disconnected crescent-shaped regions near the Fermi sphere. The boundaries of the blocking regions are the place where the dispersions in Eq. (25) are gapless.

In the d (larger) blocking region, $E_1 > 0$, $E_2 > 0$. Then,

$$E_-(\xi,\theta) = -E_1 = \delta\mu + b\cos\theta - \sqrt{\xi^2+\Delta^2},$$
$$E_+(\xi,\theta) = E_2 = \delta\mu + b\cos\theta + \sqrt{\xi^2+\Delta^2}. \quad \text{(A5)}$$

Hence,

$$\cos\theta \in \left[\min\left(\frac{-\delta\mu+\Delta}{b}, 1\right), 1\right],$$
$$\xi \in \left(-\sqrt{(\delta\mu + b\cos\theta)^2 - \Delta^2}, \sqrt{(\delta\mu + b\cos\theta)^2 - \Delta^2}\right). \quad \text{(A6)}$$

At the edge of the d blocking region, E_- is gapless. The blocking region shrinks once Δ starts to increase. Now, in the extreme limit the d blocking region vanishes at $\cos\theta = 1$. This is possible only if $\Delta/\delta\mu \sim 2.19$. In our calculations, $\Delta/\delta\mu$ is always less than 1 and hence the d blocking region never closes.

The u (smaller) blocking region is defined when $E_1 < 0$, $E_2 < 0$. Then,

$$E_-(\xi,\theta) = -\delta\mu - b\cos\theta - \sqrt{\xi^2+\Delta^2},$$
$$E_+(\xi,\theta) = -\delta\mu - b\cos\theta + \sqrt{\xi^2+\Delta^2}. \quad \text{(A7)}$$

This provides

$$\cos\theta \in \left[-1, \max\left(\frac{-\delta\mu-\Delta}{b}, -1\right)\right],$$
$$\xi \in \left(-\sqrt{(\delta\mu + b\cos\theta)^2 - \Delta^2}, \sqrt{(\delta\mu + b\cos\theta)^2 - \Delta^2}\right). \quad \text{(A8)}$$

At the edge of the u blocking region, E_+ is gapless.

The situation is opposite compared to the d blocking region. The u blocking region closes and the associated gapless surface disappears. This happens when $\Delta/\delta\mu > 0.19$ ($\delta\mu/\Delta_0 < 0.735$), which is well within the allowed regime of Δ and $\delta\mu$ (Fig. 3 in Ref. [75]).

Now, angle dependent Fermi surface splitting $\delta\mu_{\rm eff}(\cos\theta) = \delta\mu + b\cos\theta$ gives us a number of possibilities. The shape of the gapless surface as well as the nature of the gapless modes changes with the angle, $\delta\mu$ and Δ (which is a function of $\delta\mu$) [Eq. (25)] [39,72].

(i) For $\delta\mu + b\cos\theta > \Delta$, species a and b are gapless.
(ii) for $\Delta > \delta\mu + b\cos\theta > -\Delta$ all four modes are gapped.
(iii) for $\delta\mu + b\cos\theta < -\Delta$ modes c and d are gapless.
(iv) $|\delta\mu_{\rm eff}(\cos\theta)| \gg \Delta$ (in which case the dispersion near the gapless modes is linear and the mode velocity $v \approx 1$).
(v) $|\delta\mu_{\rm eff}(\cos\theta)| \approx \Delta$ (in which case the dispersion near the gapless modes is quadratic and the mode velocity $v \approx 0$).

APPENDIX B: DETAILS OF COLLISION INTEGRAL

The intermediate steps to evaluate the collision integral are presented here.

The momentum integrals in both Eqs. (10) and (11) provide dominant contributions when quasiparticles scatter near the Fermi surface. Hence, in the limit $\mu \gg \delta\mu, b, \Delta$, and $\mu \gg T$,

$$\frac{d^3p}{(2\pi)^3} = \frac{p^2 dp d\Omega}{(2\pi)^3} \approx \mu^2 d\xi \frac{d\Omega}{(2\pi)^3}. \tag{B1}$$

For both isotropic and anisotropic systems $d^3\mathbf{p}_4$ integration in the rhs of Eq. (11) is performed using the momentum δ function, which changes variables from $\mathbf{p}_3$ to $\mathbf{q} = \mathbf{p}_3 - \mathbf{p}_i = \mathbf{p}_2 - \mathbf{p}_4$. One can use the spherical symmetry to simplify the integrals further as described in Refs. [29,56] for the isotropic system to obtain

$$R_{ij}^{(n)} = -\frac{1}{\gamma^{(n)}}\frac{1}{T}\nu_2 \frac{\mu_i^2\mu_j^2}{(2\pi)^7}\int d\xi_{p_i} d\xi_{p_2} d\phi_{p_2} dq (4\pi) \int d\omega \overline{|\mathcal{M}|^2}(ij_2 \to j_3 j_4)[f_i f_2(1-f_3)(1-f_4)]$$
$$\times 3\phi_i.[\tau_i^{(n)}\psi_i^{(n)} + \tau_{j_2}^{(n)}\psi_{j_2}^{(n)} - \tau_{j_3}^{(n)}\psi_{j_3}^{(n)} - \tau_{j_4}^{(n)}\psi_{j_4}^{(n)}]|_{E_{p_3}-E_{p_i}=\omega=E_{p_2}-E_{p_4}}. \tag{B2}$$

For arbitrary $\Delta, \delta\mu, b$ the general evaluation of the collision integral R_{ij} is more difficult. When $b \neq 0$, spherical symmetry cannot be used to simplify Eq. (11). Instead of using a polar decomposition, it is simpler to write $\mathbf{q}$ in Cartesian coordinates,

$$R_{ij}^{(n)} = -\frac{1}{\gamma^{(0)}}\frac{1}{T}\nu_2 \frac{(2\pi)}{(2\pi)^9}\mu_i^2\mu_j^2 \int d\xi_{p_i} d\cos\theta_{p_i} d\phi_{p_i} d\xi_{p_2} d\cos\theta_{p_2} d\phi_{p_2} \int dq_x dq_y dq_z d\omega \overline{|\mathcal{M}|^2}(ij_2 \to j_3 j_4)$$
$$\times \delta(E_{p_3} - E_{p_i} - \omega)\delta(E_{p_4} - E_{p_2} + \omega)[f_i f_2(1-f_3)(1-f_4)]3\phi_i.[\tau_i^{(n)}\psi_i^{(n)} + \tau_{j_2}^{(n)}\psi_{j_2}^{(n)} - \tau_{j_3}^{(n)}\psi_{j_3}^{(n)} - \tau_{j_4}^{(n)}\psi_{j_4}^{(n)}]. \tag{B3}$$

To evaluate the above collision kernel we consider the direction z as the direction of the unit vector parallel to $\mathbf{b}$, p_i in the x-z plane,

$$\mathbf{p_i} = p_i(\sin\theta_{p_i}, 0, \cos\theta_{p_i}). \tag{B4}$$

This results in the integration not depending on this plane and the angular integration over ϕ_{p_i} giving a factor 2π.$\mathbf{p_2}$ is defined by the spherical coordinates,

$$\mathbf{p_2} = p_2(\sin\theta_{p_2}\cos\phi_{p_2}, \sin\theta_{p_2}\sin\phi_{p_2}, \cos\theta_{p_2}). \tag{B5}$$

We use the energy δ functions

$$\delta(E_{p_3} - E_{p_i} - \omega)\delta(E_{p_4} - E_{p_2} + \omega) \tag{B6}$$

to eliminate q_x and q_y in terms of q_z and the other variables. This is a difficult task for an anisotropic system, since in this type of system with the angle dependent dispersion relations and choices of the coordinate axes mentioned above the arguments in the δ functions involve a large number of angles. After elimination of q_x and q_y we are left with the following seven-dimensional integral:

$$R_{ij}^{(0)}\tau_j = -\frac{1}{\gamma^{(0)}}\frac{1}{T}\nu_2 \frac{(2\pi)^2}{(2\pi)^9}\mu_i^2\mu_j^2 \int d\xi_{p_i} d\cos\theta_{p_i} d\xi_{p_2} d\cos\theta_{p_2} d\phi_{p_2} dq_z \int d\omega \overline{|\mathcal{M}|^2}(ij_2 \to j_3 j_4)\frac{1}{J_q}[f_1 f_2(1-f_3)(1-f_4)]$$
$$\times 3\phi_i.[\tau_i^{(0)}\psi_i^{(0)} + \tau_{j_2}^{(0)}\psi_{j_2}^{(0)} - \tau_{j_3}^{(0)}\psi_{j_3}^{(0)} - \tau_{j_4}^{(0)}\psi_{j_4}^{(0)}]|_{E_{p_3}-E_{p_i}=\omega=E_{p_2}-E_{p_4}}. \tag{B7}$$

J_q is the Jacobian of the variable change from E to q^x and q^y.

The explicit form of J_q is given below,

$$J_q = \det\begin{pmatrix} \frac{dE_{p_3}}{d\delta\xi_{p_i}} & \frac{dE_{p_3}}{d\delta\xi_{p_2}} \\ \frac{dE_{p_4}}{d\delta\xi_{p_i}} & \frac{dE_{p_4}}{d\delta\xi_{p_2}} \end{pmatrix}\begin{pmatrix} \frac{d\delta\xi_{p_i}}{dq^x} & \frac{d\delta\xi_{p_i}}{dq^y} \\ \frac{d\delta\xi_{p_2}}{dq^x} & \frac{d\delta\xi_{p_2}}{dq^y} \end{pmatrix}, \tag{B8}$$

where

$$\delta\xi_{p_i} = \xi_{p_3} - \xi_{p_i},$$
$$\delta\xi_{p_2} = \xi_{p_4} - \xi_{p_2}, \tag{B9}$$

and

$$\frac{d\delta\xi_{p_i}}{dq^x} = \frac{p_i^x + q^x}{|p_i + q|} = \frac{p_i^x + q^x}{p_i + \delta\xi_{p_i}}. \tag{B10}$$

Finally, to evaluate the integral in Eq. (11), we need the flow part which can be expressed as follows:

$$\phi_i \cdot [\psi_i^{(0)} - \psi_{j_3}^{(0)}] = \frac{3}{4}[p_i(\cos\theta_{p_i}(v_{p_i}\cos\theta_{p_i} - \frac{1}{p_i}E_{\theta_{p_i}}\sin\theta_{p_i}) - 1/3 v_{p_i})]\Big[E_{\theta_{p_i}}((\cos\theta_{p_i} - \cos\theta_{p_3})(\sin\theta_{p_i} - \sin\theta_{p_3})) - ((p_i - p_3)(v_{p_i} - v_{p_3})(\cos^2\theta_{p_i} - \cos^2\theta_{p_3})) + \frac{1}{3}((p_i - p_3)(v_{p_i} - v_{p_3}))\Big]. \tag{B11}$$

Similarly,

$$\phi_i \cdot [\psi_{j_2}^{(0)} - \psi_{j_4}^{(0)}] = \frac{3}{2}[p_i(\cos\theta_{p_i}(v_{p_i}\cos\theta_{p_i} - \frac{1}{p_i}E_{\theta_{p_i}}\sin\theta_{p_i}) - 1/3 v_{p_i})]\Big[E_{\theta_{p_2}}((\cos\theta_{p_2} - \cos\theta_{p_4})(\sin\theta_{p_2} - \sin\theta_{p_4})) - ((p_2 - p_4)(v_{p_2} - v_{p_4})(\cos^2\theta_{p_2} - \cos^2\theta_{p_4})) + \frac{1}{3}((p_2 - p_4)(v_{p_2} - v_{p_4}))\Big], \tag{B12}$$

where $E_{\theta_{p_i}} = dE_{p_i}/d\cos\theta_{p_i}$.

We evaluate Eq. (B7) numerically with the help of Eqs. (B8), (B11), and (B12). However, to get some insight into when the Jacobian is large, it is useful to expand in the region where $\mathbf{q}$ is small.

The explicit form of J_q is given below,

$$\begin{aligned} J_q &= \det\begin{pmatrix} v_{p_i} + w_{p_i}\delta\xi_{p_i} & 0 \\ 0 & v_{p_2} + w_{p_2}\delta\xi_{p_2} \end{pmatrix}\begin{pmatrix} \frac{d\delta\xi_{p_i}}{dq^x} & \frac{d\delta\xi_{p_i}}{dq^y} \\ \frac{d\delta\xi_{p_2}}{dq^x} & \frac{d\delta\xi_{p_2}}{dq^y} \end{pmatrix} \\ &= (v_{p_i} + w_{p_i}\delta\xi_{p_i})(v_{p_2} + w_{p_2}\delta\xi_{p_2})\det\begin{pmatrix} \frac{d\delta\xi_{p_i}}{dq^x} & \frac{d\delta\xi_{p_i}}{dq^y} \\ \frac{d\delta\xi_{p_2}}{dq^x} & \frac{d\delta\xi_{p_2}}{dq^y} \end{pmatrix}. \end{aligned} \tag{B13}$$

For small q/p, q/k we obtain

$$\begin{aligned} J_q &\approx \frac{(p_i^y q^x + p_2^y(p_i^x + q^x) - p_i^x q^y - p_2^x(p_i^y + q^y))}{p_2 p_i(p_i + \delta\xi_{p_i})(p_2 + \delta\xi_{p_2})} \times (v_{p_2} + w_{p_2}\delta\xi_{p_2})((v_{p_i} + w_{p_i}\delta\xi_{p_i}) \\ &= \frac{(p_i p_2 \sin\theta_{p_i}\sin\theta_{p_2}\cos\phi_{p_2} + p_i^y q^x + p_2^y q^x - p_i^x q^y - p_2^x q^y)}{p_2 p_i(p_i + \delta\xi_{p_i})(p_2 + \delta\xi_{p_2})} \times (v_{p_2} + w_{p_2}\delta\xi_{p_2})((v_{p_i} + w_{p_i}\delta\xi_{p_i}). \end{aligned} \tag{B14}$$

In particular, we note that if v_{p_i} and v_{p_2} is small and $\delta\xi_{p_i}$ and $\delta\xi_{p_2}$ are small, then the Jacobian is small and the integral receives a large contribution.

APPENDIX C: EFFECTIVE LAGRANGIAN FOR TWO-FLAVOR PAIRING

The mean field Lagrangian for ur, ug, dr, and dg [31] quarks is given by

$$\mathcal{L} = -2\frac{\Delta^*\Delta}{\lambda} + \frac{1}{2}\Psi_{4L}^\dagger\begin{pmatrix} i\bar\sigma^\mu\partial_\mu + \mu_u & -\Delta e^{2i\mathbf{b}\cdot\mathbf{r}} \\ -\Delta^* e^{-2i\mathbf{b}\cdot\mathbf{r}} & i\sigma^\mu\partial_\mu - \mu_d \end{pmatrix}\Psi_{4L} + (L \to R), \tag{C1}$$

where

$$\Psi_{4L}(x) = \begin{pmatrix} u_L(x) \\ -[\epsilon^C]_{cc'}d_L^C(x) \end{pmatrix} \tag{C2}$$

where $[\epsilon^C]_{cc'} = \epsilon_{cc'}$ is the antisymmetric matrix in a two-dimensional subspace of color, $d_L^C(x) = (i\sigma^2)d_L^\star(x)$, and σ's are the Pauli spin matrices.

For the ur, dg quarks, it can be written as

$$\mathcal{L} = -\frac{\Delta^*\Delta}{\lambda} + \frac{1}{2}\Psi_L^\dagger\begin{pmatrix} i\bar\sigma^\mu\partial_\mu + \mu_u & -\Delta e^{2i\mathbf{b}\cdot\mathbf{r}} \\ -\Delta^* e^{-2i\mathbf{b}\cdot\mathbf{r}} & i\sigma^\mu\partial_\mu - \mu_d \end{pmatrix}\Psi_L + (L \to R), \tag{C3}$$

where $\Delta = \lambda\Theta_3$ [31] and the two-dimensional Nambu-Gorkov spinors Ψ are defined as

$$\Psi_L(x) = \begin{pmatrix} u_{rL}(x) \\ -d_{gL}^C(x) \end{pmatrix}, \quad \Psi_L^\dagger(x) = (u_{rL}^\dagger(x), -d_{gL}^{C\dagger}(x)), \tag{C4}$$

where $x=(t,\mathbf{r})$. The mean field Lagrangian for the $ug-dr$ sector has the same form as Eq. (C3). Since the contribution of the $ug-dr$ quarks is the same as that of the $ur-dg$ sector, we just focus on the $ur-dg$ quarks.

In momentum space, for $h=-1/2$, $\mathbf{p}\cdot\sigma=-p=-|\mathbf{p}|$ (this is the correct helicity for the L handed quarks). These are the large components in the Fourier decomposition of the Dirac spinor [75]. We have obtained the dispersion relations and the Bogoliubov coefficients in the main text in Sec. III C. The mode decomposition of Ψ in terms of the Bogoliubov coefficients is

$$\Psi_L(x)=\int\frac{d^4p}{(2\pi)^4}e^{-ip_\mu x^\mu}\left[(2\pi)\delta(p^0-E_1)\begin{pmatrix}\Phi_{11}e^{i\mathbf{b}\cdot\mathbf{r}}\xi_-(p)\\ \Phi_{12}e^{-i\mathbf{b}\cdot\mathbf{r}}\xi_-(p)\end{pmatrix}\gamma_L+(2\pi)\delta(p^0-E_2)\begin{pmatrix}\Phi_{21}e^{i\mathbf{b}\cdot\mathbf{r}}\xi_-(p)\\ \Phi_{22}e^{-i\mathbf{b}\cdot\mathbf{r}}\xi_-(p)\end{pmatrix}\chi_L\right],\tag{C5}$$

where ξ_- is the two component spinor satisfying

$$\mathbf{p}\cdot\sigma\xi_-(p)=-p\xi_-(p).\tag{C6}$$

The interaction can be written in terms of the Nambu-Gorkov spinors[8] as follows:

$$\begin{aligned}S_g&=g\int d^4x\bar\psi\gamma^\mu t^m\psi A^m_\mu\\&=g\int d^4x\bar\psi_L\bar\sigma^\mu t^m\psi_L A^m_\mu+g\int d^4x\bar\psi_R\sigma^\mu t^m\psi_R A^m_\mu.\end{aligned}\tag{C7}$$

Going to the momentum basis and using Eq. (C5) we obtain

$$\begin{aligned}\mathcal{L}_{AL}=&\int\frac{d^4p_i}{(2\pi)^4}\frac{d^4p_3}{(2\pi)^4}g((\Phi^*_{11}\Phi^*_{12})\gamma^\dagger_L(2\pi)\delta(p_3^0-E_1)+(\Phi^*_{21}\Phi^*_{22})\chi^\dagger_L(2\pi)\delta(p_3^0-E_2))\\&\times\begin{pmatrix}1\xi^\dagger_-(p_3)\bar\sigma^\mu\xi_-(p_i)t^m & 0\\ 0 & -1\xi^\dagger_-(p_3)C\bar\sigma^{T\mu}C^\dagger\xi_-(p_i)\epsilon_c^\dagger(t^m)^T\epsilon_c\end{pmatrix}\\&\times\left(\begin{pmatrix}\Phi_{11}\\ \Phi_{12}\end{pmatrix}\gamma_L(2\pi)\delta(p_i^0-E_1)+\begin{pmatrix}\Phi_{21}\\ \Phi_{22}\end{pmatrix}\chi_L(2\pi)\delta(p_i^0-E_2)\right)A^a_\mu(p_3-p_i),\end{aligned}\tag{C8}$$

where ϵ_c is the antisymmetric symbol in color space.

Now we can use the conjugation relation for t^1, t^2, t^3 generators,

$$-1\epsilon_c^\dagger(t^m)^T\epsilon_c=t^m,\tag{C9}$$

and the t^m gets decoupled from the Nambu-Gorkov structure. [This step does not work for the other SU(3) generators and works because the SU(2) subgroup generated by $t^1\ldots t^3$ is unbroken in two-flavor FF. See Eq. (51) for an analysis of a broken generator.] We also use the conjugation relation for $\bar\sigma^\mu$,

$$C\bar\sigma^{T\mu}C^\dagger=\sigma^\mu,\tag{C10}$$

to simplify the spin structure. This gives

$$\begin{aligned}\mathcal{L}_{AL}=&\int\frac{d^4p_i}{(2\pi)^4}\frac{d^4p_3}{(2\pi)^4}g((\Phi^*_{11}\Phi^*_{12})\gamma^\dagger_L(2\pi)\delta(p_3^0-E_1)+(\Phi^*_{21}\Phi^*_{22})\chi^\dagger_L(2\pi)\delta(p_3^0-E_2))\\&\times\begin{pmatrix}1\xi^\dagger_-(p_3)\bar\sigma^\mu\xi_-(p_i) & 0\\ 0 & 1\xi^\dagger_-(p_3)\sigma^\mu\xi_-(p_i)\end{pmatrix}\left(\begin{pmatrix}\Phi_{11}\\ \Phi_{12}\end{pmatrix}\gamma_L(2\pi)\delta(p_i^0-E_1)+\begin{pmatrix}\Phi_{21}\\ \Phi_{22}\end{pmatrix}\chi_L(2\pi)\delta(p_i^0-E_2)\right)\\&\times t^mA^m_\mu(p_3-p_i).\end{aligned}\tag{C11}$$

[8]Since we are considering the transverse gluons there are no vertex corrections.

Similarly, for R we obtain

$$\mathcal{L}_{AR} = \int \frac{d^4p_i}{(2\pi)^4}\frac{d^4p_3}{(2\pi)^4} g((\Phi^*_{11}\Phi^*_{12})\gamma^\dagger_R(2\pi)\delta(p_3^0 - E_1) + (\Phi^*_{21}\Phi^*_{22})\chi^\dagger_R(2\pi)\delta(p_3^0 - E_2)) \times \begin{pmatrix} 1\xi^\dagger_+(p)\sigma^\mu\xi_+(p) & 0 \\ 0 & 1\xi^\dagger_+(p)\bar{\sigma}^\mu\xi_+(p) \end{pmatrix} \left(\begin{pmatrix} \Phi_{11} \\ \Phi_{12} \end{pmatrix} \gamma_R(2\pi)\delta(p_i^0 - E_1) + \begin{pmatrix} \Phi_{21} \\ \Phi_{22} \end{pmatrix} \chi_R(2\pi)\delta(p_i^0 - E_2) \right) t^m A^m_\mu(p_3 - p_i). \tag{C12}$$

A nice way to separate the spinor and the Nambu-Gorkov structure is to recombine the L (C11) and R (C11) components

$$\mathcal{L}_{ALR} = \int \frac{d^4p_i}{(2\pi)^4}\frac{d^4p_3}{(2\pi)^4} g(\bar{u}_s(p_3)\gamma^\mu u_s(p_i))((\Phi^*_{11}\Phi^*_{12})\gamma^\dagger_s(2\pi)\delta(p_3^0 - E_1) + (\Phi^*_{21}\Phi^*_{22})\chi^\dagger_s(2\pi)\delta(p_3^0 - E_2)) \times \left(\begin{pmatrix} \Phi_{11} \\ \Phi_{12} \end{pmatrix} \gamma_s(2\pi)\delta(p_i^0 - E_1) + \begin{pmatrix} \Phi_{21} \\ \Phi_{22} \end{pmatrix} \chi_s(2\pi)\delta(p_i^0 - E_2) \right) t^m A^m_\mu(p_3 - p_i). \tag{C13}$$

The final ingredient we need is the simplification of the color structure in the interaction. For this we use the relation ($m = 1, 2, 3$)

$$t^m_{ij}t^m_{kl} = \left[\frac{-1}{4}\delta_{ij}\delta_{kl} + \frac{1}{2}\delta_{il}\delta_{kj}\right]. \tag{C14}$$

Summing over the final colors (j, l) and averaging over the initial colors (i, k) gives (the sum over colors runs over only two colors r and g)

$$\frac{1}{4}t^m_{ij}t^m_{kl}t^{n*}_{ij}t^{n*}_{kl} = \frac{1}{4}t^m_{ij}t^m_{kl}t^n_{ji}t^n_{lk} = \frac{3}{16}. \tag{C15}$$

APPENDIX D: CONTRIBUTION OF PHONONS

Phonons, the Goldstone modes associated with the broken symmetries, are also low energy modes. Here we make a quick estimate of their contribution to transport and to the collision integral. They are not relevant in the FF phase but play an important role in the gapped phases.

1. Quark-phonon scattering

For quark-phonon scattering, the scattering rate (Γ) is given by

$$[\Gamma_i(p_i)] = -\sum_{j_3}\int \frac{d^3l}{(2\pi)^3}\frac{d^3p_3}{(2\pi)^3}(2\pi)^4[\hat{f}_i\hat{b}_2(1-\hat{f}_3)\delta^{(4)}(p_i + l - p_3)\overline{|\mathcal{M}|^2}(il \to j_3) + \hat{f}_i(1+\hat{b}_2)(1-\hat{f}_3)\delta^{(4)}(p_i - l - p_3)\overline{|\mathcal{M}|^2}(i \to j_3 l) - \hat{f}_3\hat{b}_2(1-\hat{f}_i)\delta^{(4)}(p_i - l - p_3)\overline{|\mathcal{M}|^2}(il \to j_3) - \hat{f}_3(1+\hat{b}_2)(1-\hat{f}_i)\delta^{(4)}(p_i + l - p_3)\overline{|\mathcal{M}|^2}(il \to j_3)], \tag{D1}$$

where $\hat{f}$ and $\hat{b}$ are nonequilibrium distribution functions, and $l^\mu = (\omega, \mathbf{l})$ is the four momentum of the phonon satisfying $\omega^2 - v_\varphi^2\mathbf{l}^2 = 0$.

To the lowest order in gradient of the fluid velocity u_a, $\hat{f}_i - f_i = \delta f_i = -\frac{df^i}{d\epsilon}\Phi^i$, where

$$\Phi^i = \sum_{(n)}\Phi^{(n)}_i = \sum_{(n)} 3\tau^{(n)}_i\psi^{(n)iab}\frac{1}{2}(\partial_a u_b + \partial_b u_a). \tag{D2}$$

Substituting Eq. (D2) in the Boltzmann equation one can obtain the analogue of Eq. (11),

$$\sum_j [R_{ij}^{(n)}]\tau_j = -\frac{1}{\gamma^{(n)}}\frac{1}{T}\nu_2 \int \frac{d^3p_i}{(2\pi)^3}\frac{d^3l}{(2\pi)^3}\frac{d^3p_3}{(2\pi)^3}(2\pi)^4 3\phi_i \cdot [f_i b_2(1-f_3)\delta^{(4)}(p_i+l-p_3)(\tau_i\psi_i^{(n)})\overline{|\mathcal{M}|^2}(il\to j_3)$$
$$+ f_i(1+b_2)(1-f_3)\delta^{(4)}(p_i-l-p_3)(\tau_i\psi_i^{(n)})\overline{|\mathcal{M}|^2}(i\to j_3 l)$$
$$- f_3 b_2(1-f_i)\delta^{(4)}(p_i-l-p_3)(\tau_3\psi_3^{(n)})\overline{|\mathcal{M}|^2}(i\to j_3 l)$$
$$- f_3(1+b_2)(1-f_i)\delta^{(4)}(p_i+l-p_3)(\tau_3\psi_3^{(n)})\overline{|\mathcal{M}|^2}(il\to j_3)], \tag{D3}$$

where b is the Bose distribution.

The scattering matrix element associated with the vertex in Eq. (41) is given by

$$\overline{|\mathcal{M}|^2} \sim |\frac{i}{f_\varphi^{ij}}\frac{1}{\sqrt{2\omega}\sqrt{2p_i}\sqrt{2p_3}}|^2 4c^2[2p_i\cdot l p_3\cdot l - p_i\cdot p_3 l^2]|$$
$$\sim \frac{l^2}{(f_\varphi^{ij})^2\omega} \sim \frac{\omega}{(f_\varphi^{ij})^2} \tag{D4}$$

where we have taken $c_0 \sim c'$ to simplify the argument.

Simplifying the momentum integrals for the fermions (d^3p_i and d^3p_3) as in Eq. (B1), noting that ξ_i, ξ_3 and ω are all of the order of T, and that ϕ and ψ are of the order of μ, we can see without evaluating the integrals that

$$[R_{(q-\mathrm{ph})ij}] \sim c^2\frac{\mu^3T^4}{(f_\varphi^{ij})^2} \sim \mu T^4, \tag{D5}$$

where we have used a rough estimate for f_φ: $f_\varphi \sim \mu$.

When unpaired quarks participate in transport and T is much less than the chemical potential μ, the contribution from Eq. (D5) is subleading compared to the collision term associated with quark-quark scattering in Eq. (E5). This is simple to understand because the density of states for gapless fermions near the Fermi surface is proportional to μ^2 while the density of states of phonons is proportional to T^2. We see in Sec. E 2 a that this is not true for paired systems with no gapless fermions.

2. Momentum transport via phonons

If phonons are present in the low energy theory then they can also transport energy and momentum. While this is not the main topic of the paper, we make a quick estimate to see how this contribution compares with the fermionic contribution.

The kinetic theory estimate for the shear viscosity of the phonon gas is

$$\eta \sim \langle n\rangle\langle p\rangle v_\varphi \tau_\varphi. \tag{D6}$$

The density of phonons at temperature T is given by $\langle n\rangle \sim \frac{T^3}{v_\varphi^3}$ and $\langle p\rangle \sim \frac{T}{v_\varphi}$. Consequently,

$$\eta \sim \frac{1}{v_\varphi^3}T^4\tau_\varphi. \tag{D7}$$

τ_φ is very sensitive to the nature of the excitations present in the low energy theory. For example, if all the fermionic modes are gapped, then the phonons only scatter with each other. Since the phonons are coupled derivatively, the relaxation time in these cases is very long due to the small density of phonons at low temperatures, and hence the viscosity is very large. It is well known that in the absence of gapless fermions these phonons dominate the viscosity at low T (Refs. [96,97]).

For example, if the dominant scattering rate is $2\to 2$ scattering then the shear viscosity is given by [98,99]

$$\eta \sim \frac{1}{v_\varphi^3}\frac{f_\varphi^8}{T^5}. \tag{D8}$$

In both the unpaired phase and in the FF phase, phonons can scatter off gapless fermionic excitations which have a large density of states near the Fermi surface. This effect is simply the Landau damping of the phonons. The scattering rate of the phonons is $\Gamma \sim 1/\tau \sim \frac{\mu^2}{f_\varphi^2}T$ [100]. A quick estimate gives

$$\eta \sim \frac{1}{v_\varphi^3}\frac{f_\varphi^2}{\mu^2}T^3, \tag{D9}$$

which is much smaller than Eq. (E6) for $T \ll \mu$.

APPENDIX E: RESULTS FOR A SIMPLE INTERACTION FOR ISOTROPIC PAIRING

1. Unpaired fermions

In this section we review well-known results for the shear viscosity of the unpaired phase and then show new results on how the shear viscosity is modified due to (1) gapped pairing in Appendix E 2 a, (2) gapless pairing in Appendix E 2 b, and (3) FF pairing in Sec. IV.

In this section we focus on the scattering via the longitudinal A_μ, with an interaction of the form in Eq. (47). We approximate the polarization tensor of the

longitudinal mode of A_μ by the Debye screened mass [Eq. (49) with $N_f = 1$]. The matrix element for the scattering of quarks by the longitudinal A_μ is given by Eq. (50).

We note that Eq. (50) is nothing but the Möller scattering of identical particles. In this scenario $\mathcal{M}$ has two parts $i \to j_2, j_3 \to j_4$ and $i \to j_4, j_2 \to j_3$. Hence, after squaring there appear three term squares of these two contributions as well as their interference term. However, in the limit of small momentum transfer the interference term gives small contribution and hence can be excluded [56,101]. The other two terms give equal contributions.

The dispersions are given by Eq. (25) with $b = 0, \Delta = 0$. Dropping the absolute sign in ξ, $E = \delta\mu \pm \xi$ and we do not need to distinguish between the $\xi > 0$ and $\xi < 0$ modes. For convenience here we can put $\delta\mu = 0$ and the two species can be treated as identical. (The corrections to the results are suppressed by $\delta\mu/\mu$.)

In this case the lhs of Eq. (10) is simply given by the integral,

$$L_1^{\rm un} = \frac{1}{\gamma^{(n)}}\frac{2\pi\mu^2}{(2\pi)^3}\frac{1}{T}\int_{-\infty}^{\infty} d\xi \frac{1}{(e^{\xi/T}+1)}\frac{1}{(e^{-\xi/T}+1)} \times \int d\cos\theta \mu^2 \frac{3}{2}\left(\cos^2\theta - \frac{1}{3}\right)^2. \tag{E1}$$

Using $\gamma^{(0)} = 1$, we obtain

$$[L_i^{\rm un}] = \begin{pmatrix} -\frac{4}{15}\frac{\mu^4}{(2\pi)^2} & \\ & -\frac{4}{15}\frac{\mu^4}{(2\pi)^2} \end{pmatrix}. \tag{E2}$$

(We use the superscript "un" to denote the values of L_i, R_{ij}, τ and η for one unpaired species with the dispersion relation $E = \xi$.)

The rhs of Eq. (11) can be obtained following Refs. [29,56]. The interaction mentioned in Eq. (47) does not change flavor, and hence the species index j_3 is the same as i, and j_2 is the same as j_4. There are two relevant integrals which give

$$s_1^{\rm un} = -\frac{1}{\gamma^{(n)}}\frac{1}{T}\nu_2 \int \frac{d^3p_i}{(2\pi)^3}\frac{d^3p_2}{(2\pi)^3}\frac{d^3p_3}{(2\pi)^3}\frac{d^3p_4}{(2\pi)^3}\overline{|\mathcal{M}|^2}(ij_2 \to j_3 j_4)(2\pi)^4\delta\left(\sum p^\mu\right)[f_i f_2(1-f_3)(1-f_4)]3\phi_i.[\psi_i^{(n)} - \psi_3^{(n)}]$$
$$\approx -\nu_2 \frac{g^4}{16\cdot 5}\frac{\pi^3}{(2\pi)^5}\frac{\mu^4 T^2}{\sqrt{\Pi_l(0)}}$$
$$s_2^{\rm un} = -\frac{1}{\gamma^{(n)}}\frac{1}{T}\nu_2 \int \frac{d^3p_i}{(2\pi)^3}\frac{d^3p_2}{(2\pi)^3}\frac{d^3p_3}{(2\pi)^3}\frac{d^3p_4}{(2\pi)^3}\overline{|\mathcal{M}|^2}(ij_2 \to j_3 j_4)(2\pi)^4\delta\left(\sum p^\mu\right)[f_i f_2(1-f_3)(1-f_4)]3\phi_i.[\psi_2^{(n)} - \psi_4^{(n)}]$$
$$\approx 0. \tag{E3}$$

The analytic approximations for the collision integrals are obtained by assuming the integral is dominated by momentum exchanges $q \ll \mu$. (Only an interference between the transverse and the longitudinal gauge field exchange contributes to s_2.) From the form of the gluon propagator [Eq. (48)] one can argue that the typical momentum exchange is

$$q \sim m_D = \frac{\sqrt{N_f} g\mu}{\pi}. \tag{E4}$$

For strong coupling (we draw the plots for $\alpha_s = 1$) $m_D \ll \mu$ is not satisfied. In the numerical calculation we do not approximate $q \ll \mu$. We find that the expressions given in Eq. (E3) considering $q \ll \mu$ are accurate within 30% to the numerical estimate for the interaction mentioned in Eq. (51), and more importantly it has the correct scaling behavior with μ and T.

The matrix R_{ij} is related to $s^{\rm un}$ by

$$[R_{ij}^{\rm un}] = \begin{pmatrix} (2s_1^{\rm un} + s_2^{\rm un}) & s_2^{\rm un} \\ s_2^{\rm un} & (2s_1^{\rm un} + s_2^{\rm un}) \end{pmatrix} \approx -\frac{g^3 T^2 \mu^3 \nu_2}{640\pi\sqrt{2}}\begin{pmatrix} 1 & 0 \\ 0 & 1 \end{pmatrix}. \tag{E5}$$

Equations (E2) and (E5) can be used to compute the viscosity for unpaired quarks with which we can compare the results of the paired system. In the approximation $q \ll \mu$ one obtains

$$\tau_1^{\rm un} = \tau_2^{\rm un} = \frac{L_1^{\rm un}}{2s_1^{\rm un}} \approx \frac{256\sqrt{\Pi_l(0)}}{3\nu_2 g^4 T^2} = \frac{128\sqrt{2}\mu}{3g^3\pi T^2 \nu_2},$$
$$\eta_1^{\rm un} = \eta_2^{\rm un} = -\frac{3}{2}\nu_2 L_1^{\rm un}\tau^{\rm un} \approx \frac{128\sqrt{\Pi_l(0)}\mu^4}{15 g^4\pi^2 T^2} \approx \frac{64\sqrt{2}\mu^5}{15 g^3 \pi^3 T^2}. \tag{E6}$$

The total viscosity of the system is

$$\eta^{\rm un} = \eta_1^{\rm un} + \eta_2^{\rm un} = 2\eta_1^{\rm un}. \tag{E7}$$

Typically the system described above features additional low energy modes. For example, to ensure the neutrality of the system a background of oppositely charged particles is necessary, and fluctuations in their density are gapless. (A real world example is the electron gas in a lattice of ions.) Quarks can scatter off these phonons. In Sec. D 1 we made a quick estimate of how these processes affect quark transport and found that $R_{ij}^{\text{q-ph}} \sim \mu T^4$, which is parametrically smaller than Eq. (E5). Therefore they can be ignored for unpaired quark matter. However, these scattering processes turn out to be important in the next section.

Finally, it is easy to see that the viscosity contribution of unpaired quarks [Eq. (E6)] is much larger than the contribution of phonons in the presence of unpaired quarks [Eq. (D9)].

a. Results for transverse gluon exchange for unpaired quarks

For completeness we review results for the shear viscosity when the dominant quark-quark interaction is the exchange of the Landau damped transverse gluons. In principle, both the longitudinal and the traverse gluon exchanges are present and can interfere, but for most parameters one dominates over the other and they can be treated separately.

The lhs of the Boltzmann equation [Eq. (10)] is independent of interactions and hence L_i is given by Eq. (E2) regardless of whether the longitudinal or the transverse gluons dominate.

For isotropic Landau damping [Eqs. (31) and (32) for three Landau damped gluons t^1, t^2, and t^3 with $N_f = 2$], a rough estimate [29,56] for R_{ij} is given by

$$\frac{R_{11}^{t\rm un}}{R_{11}^{\rm un}} \approx \frac{3}{2^{1/6}} \left(\frac{g\mu}{\pi^2 T}\right)^{1/3}, \tag{E8}$$

where $R_{11}^{\rm un}$ is calculated with the longitudinal interaction given in Eq. (E5) and $R_{11}^{t\rm un}$ is for the transverse interaction.

Just like Eq. (E3), we find that the analytic estimate in Eq. (E8) for R_{ij} is accurate within 30% for the interaction given by Eqs. (31) and (32), in the range of parameters we have explored. It also captures the correct scaling behavior with μ and T.

Equation (E8) is the explicit manifestation of the result mentioned in Sec. II. If present, the Landau damped transverse gluon exchange dominates over the longitudinal gluon exchange in unpaired quark matter at low T: the ratio in Eq. (E8) is much larger than 1 for $T \ll \mu$.

With the collision integral R_{ij} in hand, we can calculate τ and η. We obtain

$$\frac{\tau_1^{t\rm un}}{\tau_1^{\rm un}} \approx \frac{2^{1/6}}{3} \left(\frac{g\mu}{\pi^2 T}\right)^{-1/3}, \tag{E9}$$

and

$$\frac{\eta_1^{t\rm un}}{\eta_1^{\rm un}} \approx \frac{2^{1/6}}{3} \left(\frac{g\mu}{\pi^2 T}\right)^{-1/3}. \tag{E10}$$

Equations (E8)–(E10) are compared with results for the FF phase in Sec. IV B. In both cases the dominant gluon exchange is the Landau damped transverse gluon exchange. But in the FF phase the dispersion of the quarks is given by Eq. (25) and this has an important impact.

2. Paired fermions

We now consider the effect of the isotropic pairing ($b = 0$) on transport to get some intuition into the anisotropic problem. In the isotropic systems we can simplify the integrals R_{ij} [Eq. (11)] using rotational symmetry. In Sec. E 2 a we take $\delta\mu = 0$ and see how pairing affects the fermionic contribution to the viscosity. In Sec. E 2 b we take $\delta\mu \neq 0$ and see how the gapless modes that arise when $\Delta < \delta\mu$ contribute to transport. In the FF phase, the fermions at the boundary of the blocking regions are gapless and we expect to see that they share some features of the system considered in Sec. E 2 b.

a. Bardeen-Cooper-Schrieffer pairing

For $\delta\mu = 0$ the transport properties depend on the three dimensionful quantities μ, T, and Δ. The overall scale is set in terms of the chemical potential μ. The quantities L_i/μ^4, R_{ij}/μ^5, $\tau\mu$ and η/μ^3 are dimensionless and can be written as functions of the variables $(\frac{T}{\mu}, \frac{\Delta}{\mu})$. The analysis is further simplified by the observation that we can write the quantities of interest as a result of unpaired quark matter multiplied by a function only of Δ/T [e.g. see Eq. (E11)].

The effect of pairing is shown in Fig. 8 where we present how the transport properties change from their values in unpaired quark matter as we increase Δ/T. Below, we describe the behavior in various limiting cases as we change Δ/T. For isotropic systems the phase space integral [Eq. (B2)] can be evaluated numerically with a high accuracy and the errors in the solid curves of Fig. 8 are comparable to their thickness.

$\Delta \ll T$: When the pairing parameter $\Delta \to 0$ (see Fig. 8), we get back a system of unpaired fermions and one should obtain the result in Sec. E 1 in the language of the Bogoliubov quasiparticles [Eq. (26)].

L_i is given by half the values given in Eq. (E2) [the factor of $1/2$ arises because we restrict the integrals in ξ to $\xi > 0$ or < 0 corresponding to Eq. (26)],

$$[L_i](\Delta = 0) = \frac{1}{2} L_1^{\rm un}(1,1,1,1). \tag{E11}$$

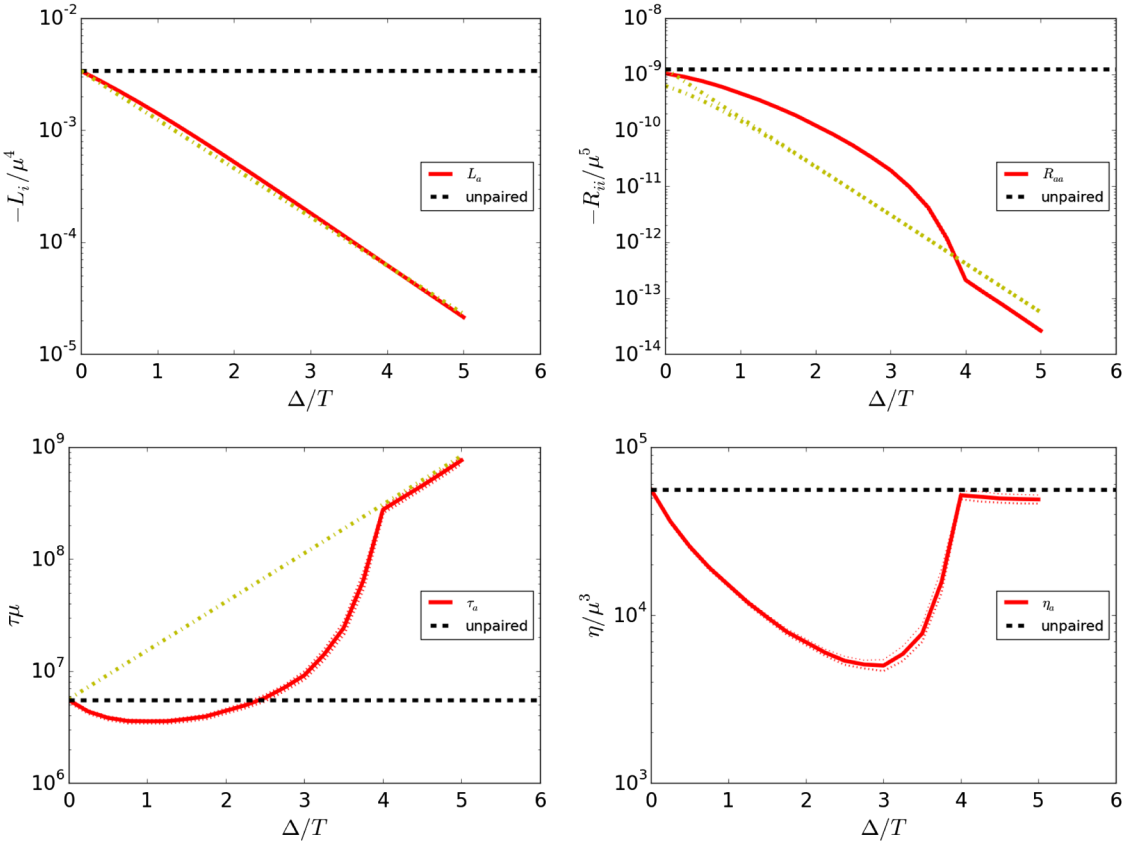

FIG. 8. Plots of L_i, the diagonal entries of R_{ij}, η_i and τ_i (anticlockwise from top left) for paired quark matter for $\overline{|\mathcal{M}|^2}$ given in Eq. (51). The results for all four species a, b, c, d are identical and shown by the solid curve (red online). The overall scale is set by $\mu.T/\mu = 3.34 \times 10^{-4}$ is held fixed and $\delta\mu = 0$. The dot dashed curves (yellow online) show an exponential fall off, $\propto \exp(-\Delta/T)$, for L_i [Eq. (E14)], an exponential fall off $\propto \exp(-2\Delta/T)$, for R_{ii} [Eq. (E15)], and an exponential increase, $\propto \exp(\Delta/T)$, for τ_i. The horizontal dashed curves (black online) for L_i [R_{ij}, τ, η] correspond to $L^{\rm un}/2$ [Eq. (E2)], $R_{11}^{\rm un}$ [Eq. (E5)], $\tau_1^{\rm un}$ and $\eta_1^{\rm un}/2$ [Eq. (E6)].

For the collision integral, we numerically find that to a high accuracy the matrix R_{ij} has the form

$$R_{ij}(\Delta = 0) = 2s_1^{\rm un}\begin{pmatrix} \frac{1}{2}+\mathrm{f}_2\left(\frac{T}{\mu},\frac{1}{g}\right) & 0 & 0 & \frac{1}{2}-\mathrm{f}_2\left(\frac{T}{\mu},\frac{1}{g}\right) \\ 0 & \frac{1}{2}+\mathrm{f}_2\left(\frac{T}{\mu},\frac{1}{g}\right) & \frac{1}{2}-\mathrm{f}_2\left(\frac{T}{\mu},\frac{1}{g}\right) & 0 \\ 0 & \frac{1}{2}-\mathrm{f}_2\left(\frac{T}{\mu},\frac{1}{g}\right) & \frac{1}{2}+\mathrm{f}_2\left(\frac{T}{\mu},\frac{1}{g}\right) & 0 \\ \frac{1}{2}-\mathrm{f}_2\left(\frac{T}{\mu},\frac{1}{g}\right) & 0 & 0 & \frac{1}{2}+\mathrm{f}_2\left(\frac{T}{\mu},\frac{1}{g}\right) \end{pmatrix} \tag{E12}$$

[with $s_2^{\rm un} = 0$ and $s_1^{\rm un}$ given in Eq. (E3)].

The structure of the matrix in Eq. (E12) is easy to understand. The diagonal entries correspond to the scattering of species i with i. For $\Delta = 0$ the branch a is connected to d and b to c, and these scattering contributions are finite and they add up to $2s_1^{\rm un}$. In a wide range of $T \ll \mu$, $\mathrm{f}_2(\frac{T}{\mu},\frac{1}{g})$ is relatively insensitive to T/μ and increases with increasing $\frac{1}{g}$ (weak coupling). This is because $\mathrm{f}_2(\frac{T}{\mu},\frac{1}{g})$ is related to the scatterings between a and d (or b and c) species and the interactions are more pronounced at small angles ($q \sim g\mu \ll \mu$). This indeed signifies that smaller g provides the dominant effect. The contribution to the collisional integral from scattering of particles in the branch a with b or c is 0 from rotational symmetry [just like $s_2^{\rm un} = 0$ in Eq. (E3)].

From Eqs. (E11) and (E12) one can easily obtain relaxation time $\tau_i(\Delta = 0) = \tau_1^{\rm un}$ and hence the shear

viscosity is $\eta_i = \frac{1}{2}\eta_1^{\rm un}$ for all four species. The total viscosity is given by

$$\eta(\Delta = 0) = \sum_i \eta_i(\Delta = 0) = 4\eta_i(\Delta = 0) = 2\eta_1^{\rm un}. \quad \text{(E13)}$$

The dashed horizontal line (black online) on the top left panel of Fig. 8 corresponds to $L_i = \frac{1}{2}L_1^{\rm un}$ [Eqs. (E2) and (E11)]. The dashed horizontal lines (black online) on the top right panel of Fig. 8 correspond to $R_{11}^{\rm un} = 2s_1^{\rm un}$ [Eqs. (E5) and (E12)]. For the parameters of Fig. 8 the numerical result [shown in the top right panel of Fig. 8 by the dashed horizontal line (black online)] for $R_{11}^{\rm un}/\mu^5 = -1.23 \times 10^{-9}$. The analytic expression [Eq. (E3)] gives $R_{11}^{\rm un}/\mu^5 = -9.8 \times 10^{-10}$. The dashed horizontal line (black online) on the bottom left and on the bottom right panel of Fig. 8 corresponds to τ_i and η_i [Eq. (E6)] for unpaired quarks, respectively.

$\Delta \gg T$: As Δ increases, the participation of fermions in transport starts to get thermally suppressed. Since the L_i's involve single particle excitations, it is easy to see that

$$L_i(\Delta) \approx L_i(\Delta = 0)e^{-\Delta/T}. \quad \text{(E14)}$$

This is shown by the dot dashed curve (yellow online) in Fig. 8.

Similarly, since the R_{ij}'s involve two particle excitations, we expect that

$$R_{ij}(\Delta) \sim R_{ij}(\Delta = 0)e^{-2\Delta/T}. \quad \text{(E15)}$$

This is shown by the dot dashed curve (yellow online) in Fig. 8. We see in Fig. 8 that this exponential drop in R_{ij} turns out to be true for Δ/T larger than 4 and the suppression in R_{ij} for $\Delta/T \lesssim 4$ while present is a little weaker as we discuss below.

$\Delta \lesssim 4T$: While Eq. (E14) gives a good description of L_i for all Δ/T, the behavior of R_{ij} in the intermediate regime is a little more complicated. For $\Delta \lesssim 4T$,

$$|R_{ij}(\Delta)| > |R_{ij}(\Delta = 0)|e^{-2\Delta/T}. \quad \text{(E16)}$$

This is because pairing opens up processes that are forbidden in unpaired quark matter. For example, a process $i = a$, $j_2 = c$, $j_3 = c$, $j_4 = d$ is 0 in unpaired quark matter because gluons cannot change the flavor of the quark. But in the presence of pairing, finite Bogoliubov coefficients [Eqs. (21) and (22)] allow such processes. At large enough Δ, these processes turn off but in the intermediate regime they display a nonmonotonic behavior. This bump in R_{ij} is reflected in τ and shows up as a minimum in η at $\Delta/T \approx 3$.

We note that the transition from the $\Delta \lesssim 4T$ regime to the $\Delta \gg T$ behavior seems abrupt, almost like a kink in R_{ij}. We think it is simply because of the sharp exponential turn off of these processes near $\Delta \approx 4T$ and is not associated with any transitions.

Focusing on $\Delta \gg T$, Eq. (E15) is a reflection of the fact that few thermally excited quarks scatter with each other. The large relaxation time compensates for the small number of momentum carrying fermions and for $\Delta/T \gtrsim 4$ the viscosity converges back to the value for unpaired quark matter as can be seen in the bottom right panel of Fig. 8 (η) where we see that after reaching a minimum near $\Delta/T \approx 3$, η rises again and flattens near the value for unpaired quark matter.

This result is puzzling since we expect the paired fermions to be frozen at temperatures smaller than the pairing gap. We expect only the low energy phonons to participate in transport at low energies [98].

We argued in the previous section (Sec. E 1) that in the absence of pairing for $T \ll \mu$, the contribution to the quark collision integral R_{ij} from quark-phonon scattering [Eq. (D5)] is subdominant to the contribution from quark-quark scattering [Eq. (E5)]. Pairing, however, affects these two contributions differently. Since quark-phonon scattering involves only one gapped mode, we expect the $R_{ij(q-\rm ph)}(\Delta) \sim R_{ij(q-\rm ph)}(0)e^{-\Delta/T}$ rather than $\sim e^{-2\Delta/T}$ [Eq. (E15)] and hence dominates scattering. Then τ_i does not grow exponentially and η_i is exponentially suppressed.

More systematically, for $\Delta \gg T$,

$$L_i \approx \frac{-2}{15}\frac{\mu^4}{(2\pi)^2}e^{-\Delta/T}, \qquad i = a, b, c, d \quad \text{(E17)}$$

and [Eqs. (E15) and (D5)]

$$\begin{aligned} R_{ii}(\Delta) &\approx \left[-\frac{1}{2}\frac{g^3T^2\mu^3\nu_2}{640\pi\sqrt{2}}e^{-2\Delta/T} - c\mu T^4 e^{-\Delta/T}\right] \\ &\approx -c\mu T^4 e^{-\Delta/T} \quad i = a, b, c, d \end{aligned} \quad \text{(E18)}$$

where we have taken $\Pi_l(0) = (g\mu/(2\pi))^2$ and c is a number $\mathcal{O}(1)$. Hence,

$$\tau_i \approx \frac{2c}{15(2\pi)^2}\frac{\mu^3}{T^4} \quad i = a, b, c, d. \quad \text{(E19)}$$

Therefore, the fermionic contribution to the shear viscosity is given by

$$\eta_i = -3\tau_i L_i \approx \frac{4}{75(2\pi)^4}\frac{\mu^7}{T^4}e^{-\Delta/T} \quad i = a, b, c, d, \quad \text{(E20)}$$

which is subdominant to the phonon contribution [Eq. (D8)], since we are assuming no other gapless fermions are present.

The argument from Eqs. (E17)–(E20) for the dominance of phonons to describe the transport properties in a paired system relies on the existence of a gapless Goldstone mode in the low energy theory. (A similar

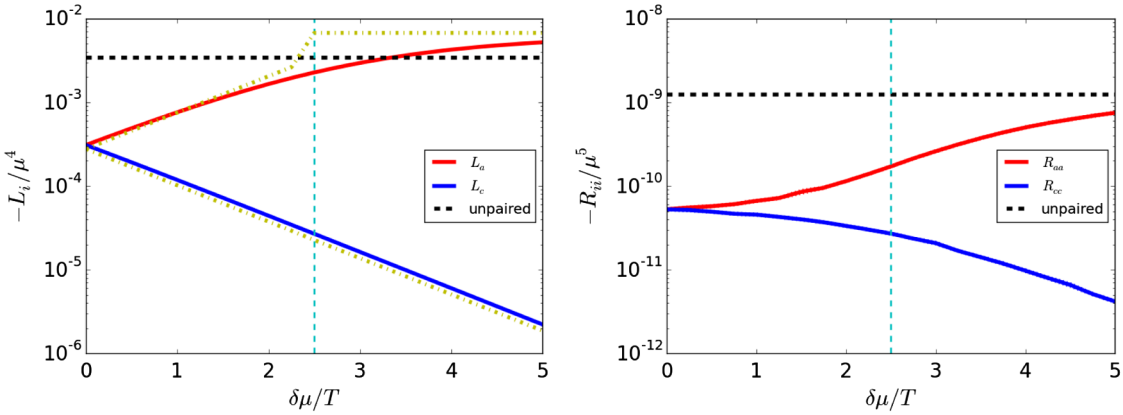

FIG. 9. Plots of L_i (left) and the diagonal entries of R_{ij} (right) with $\overline{|\mathcal{M}|^2}$ given in Eq. (51). The dashed horizontal lines correspond to the values for unpaired matter. $T/\mu = 3.34 \times 10^{-4}$ and $\Delta/T = 2.5$ are held fixed. The dot dashed curves (yellow online) for L_i are the simple forms given in Eq. (E22) for $\delta\mu > \Delta$, and Eq. (E21) for $\delta\mu < \Delta$. The results [upper solid curves (red online)] for a are the same as b as both become gapless for $\delta\mu > \Delta$. The results [lower solid curves (blue online)] for c are the same as d as both remain gapped for $\delta\mu > \Delta$. The dashed vertical line (cyan online) corresponds to Δ/T and separates the gapped (left) and the gapless (right) regimes.

argument holds if there are additional unpaired or gapless fermions that couple to the paired fermions.) In most of the paired systems we know such a mode is present. If the symmetry broken by the fermion condensate is global or has a global component,[9] then the pairing itself gives rise to a Goldstone mode which can scatter off fermions. If the symmetry broken by the condensate is local rather than global, then pairing does not give rise to a phonon mode. For example in ordinary Bardeen-Cooper-Schrieffer superconductors the local $U(1) \to Z_2$ gives a mass to the transverse photons (the Meissner effect). However even in this case there is a Goldstone mode associated with the breaking of translational symmetry by the underlying lattice.[10]

Therefore the common statement that the paired fermions do not contribute to transport at low temperatures is generically true, but subtle. Things are cleaner if there are fermionic modes that are gapless, in which case they dominate transport when $\mu \gg T$. This is the situation we explore in the next section.

In drawing Fig. 8 we have taken $\alpha_s = 1$. Obtaining results for arbitrary g is simple. The square of the matrix element, $\overline{|\mathcal{M}|^2}$, scales as g^4 and $\sqrt{\Pi_l}$ scales as g. Consequently τ_i and η_i scale as $1/g^3$.

[9]For quark pairing the condensate breaks baryon number conservation. For cold atoms fermion number conservation is a global symmetry. In both these cases the dispersion of the resultant mode is $v_F/\sqrt{3}$ and hence absorption of phonons by fermions is kinematically allowed.

[10]The sound speed of the lattice phonons is much smaller than the Fermi speed of the fermions and fermion phonon scattering is kinematically allowed. However hypothetically one can consider a situation when this is not the case. Then the statement that gapped contributions do not contribute to transport will not hold. Since this is not germane to our paper we do not explore this further here.

b. Isotropic gapless pairing

In this section we analyze the isotropic gapless paired phase which includes $\delta\mu$ in the dispersion relation i.e. the dimensionful scales obey $\mathbf{b} \to 0$, $\Delta > \delta\mu$. As discussed in Sec. II, this phase is unstable, but the analyses give us insight into the anisotropic calculation.

For $\delta\mu$ nonzero, L_i/μ^4, R_{ij}/μ^5, $\tau\mu$, and η/μ^3 are functions of the variables $(\frac{T}{\mu}, \frac{\Delta}{\mu}, \frac{\delta\mu}{\mu})$. The analysis is further simplified by assuming that we can write the quantities of interest as the result for unpaired quark matter [Eqs. (E2), (E5), and (E6)] multiplied by a function only of $(\Delta/T, \delta\mu/T)$ [e.g. see Eqs. (E21) and (E22)]. This approximate ansatz gives insight into the behavior of the transport properties in the regime $\delta\mu > \Delta$ as shown below.

Exploring the full dependence of L_i and R_{ij} on $(\Delta/T, \delta\mu/T)$ is not be very useful for us here. The key feature we want to understand here is how the properties of gapped ($\Delta > \delta\mu$) and gapless ($\Delta < \delta\mu$) phases differ. To this end, we fix Δ/T, and vary $\delta\mu$ to go from the gapped to the gapless regime.

Based on the discussion in the previous section (Sec. E 2 a), we expect that for $\Delta > \delta\mu$ both the lhs and the rhs of the Boltzmann equation will be exponentially suppressed from the unpaired value and behave like a system of gapped fermions. Increasing the value of $\delta\mu$ alters the situation. For $\Delta < \delta\mu$ from Eq. (24) it can be seen that the branches a and b in Eq. (26) becomes gapless while the branches c and d remain gapped.

The region to the left of $\delta\mu/T = 2.5$ (vertical dashed line in Fig. 9) corresponds to $\Delta > \delta\mu$ where all fermionic excitations are gapped and all components of R_{ij} are exponentially suppressed. For the regime $\delta\mu/T > 2.5$, $\Delta < \delta\mu$, branches a and b feature gapless fermionic excitations. The asymptotic value ($\delta\mu \gg \Delta$) converges to $\eta_a = \eta_b = 2\eta_1^{\rm un}$.

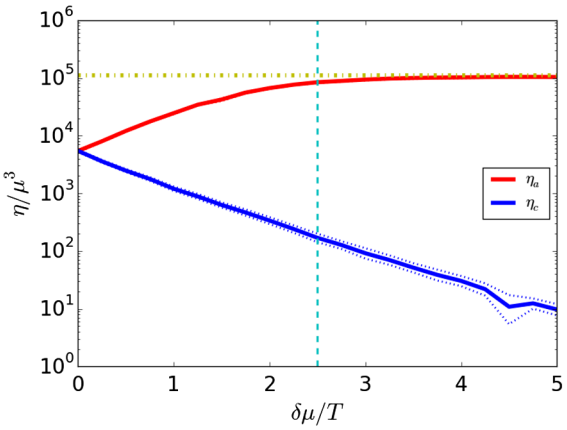

FIG. 10. Plot of $\eta_a = \eta_b$ [the upper solid curve (red online)] and $\eta_c = \eta_d$ [the lower solid curve (blue online)] from the results of Fig. 9. The dot-dashed curve (yellow online) shows $\eta_1^{\rm un}$.

More specifically, for $\Delta - \delta\mu \gg T$

$$L_{a,b}(\Delta,\delta\mu) \approx \frac{1}{2} L_1^{\rm un} e^{-\frac{(\Delta-\delta\mu)}{T}} = L_a(\Delta=0,\delta\mu=0) e^{-\frac{(\Delta-\delta\mu)}{T}},$$
$$L_{c,d}(\Delta,\delta\mu) \approx \frac{1}{2} L_1^{\rm un} e^{-\frac{(\Delta+\delta\mu)}{T}} = L_a(\Delta=0,\delta\mu=0) e^{-\frac{(\Delta+\delta\mu)}{T}}. \tag{E21}$$

The splitting between gapless and gapped species increases as we increase $\delta\mu$. For $\delta\mu - \Delta \gg T$, near the gapless surfaces $\xi = \pm\sqrt{\delta\mu^2 - \Delta^2}$, both a and b branches resemble unpaired fermions. Therefore,

$$L_{a,b}(\Delta,\delta\mu)_{\delta\mu\gg\Delta} \to L_1^{\rm un} = 2L_a(\Delta=0,\delta\mu=0)$$
$$L_{c,d}(\Delta,\delta\mu) \approx \frac{1}{2} L_1^{\rm un} e^{-\frac{(\Delta+\delta\mu)}{T}}. \tag{E22}$$

Similarly, for $\Delta - \delta\mu \gg T$ we expect R_{ii} for each i to be suppressed compared to $R_{ii}^{\rm un}$. For example, for $\delta\mu = 0$, we see that for $\Delta/T = 2.5$, $R_{ii}(\Delta = 2.5T, \delta\mu = 0) \approx R_{ii}^{\rm un}/15$. The suppression factor of 15 is consistent with the same factors in Fig. 8.

As $\delta\mu$ is increased, the gapless branches a, b split from c and d, and eventually for $\delta\mu - \Delta \gg T$

$$R_{aa,bb}(\Delta,\delta\mu)|_{\delta\mu\gg\Delta} \to R_{11}^{\rm un}$$
$$R_{cc,dd}(\Delta,\delta\mu) \sim R_{11}^{\rm un} \exp(-2(\Delta+\delta\mu)/T). \tag{E23}$$

The off-diagonal terms of R_{ij} are also exponentially suppressed.

This pattern is repeated for τ and η. For $(\delta\mu - \Delta) \gg T$ $\tau_{a,b}$ ($\eta_{a,b}$) tend towards $\tau_1^{\rm un}$ ($\eta_1^{\rm un}$) while $\tau_{c,d}$ ($\eta_{c,d}$) are exponentially suppressed. The results for η are shown in Fig. 10 and show that $\eta^a = \eta^b = \eta_1^{\rm un}$.

All these are just a complicated way to obtain the well-understood result Ref. [102] that transport in gapless

TABLE II. Summary of unpaired, paired, isotropic gapless and FF phases.

	Unpaired	Paired	Isotropic gapless	Anisotropic (Debye)	Anisotropic (Landau)
Dispersions	$E=\lvert p\rvert$	$E=\sqrt{\xi^2+\Delta^2}$	$E=\delta\mu\pm\sqrt{\xi^2+\Delta^2}(\delta\mu>\Delta)$	$E=\delta\mu+b\cos\theta \pm\sqrt{\xi^2+\Delta^2}$	Like Debye
lhs	$L_i\propto\mu^4$	$L_i\sim L^{\rm un}\times e^{-\Delta/T}$	$L_{a,b}\sim L^{\rm un},(\delta\mu-\Delta\gg T)$	$L_{a,b}\sim L^{\rm un}\times\frac{1}{2}(1+\frac{\delta\mu}{b}-\frac{\Delta}{b})$	
			$L_{c,d}\propto L^{\rm un}e^{-\frac{(\Delta+\delta\mu)}{T}}$	$L_{c,d}\sim L^{\rm un}e^{-\frac{\Delta}{T}}$	Like Debye
rhs	$R_{11}\propto T^2\mu^3$	$R_{ij}\sim R_{11}^{\rm un}e^{-2\Delta/T}$, $(\Delta\gg T)$	$R_{aa,bb}\sim R_{11}^{\rm un},(\delta\mu-\Delta\gg T)$	$R_{aa,bb}\sim\frac{1}{2}R_{11}^{\rm un}$ $\times\frac{1}{4}(1+\frac{\delta\mu}{b}-\frac{\Delta}{b})^2$	$R_{aa,bb}\sim 10^2 R_{11}^{\rm run}$
			$R_{cc,dd}\sim R_{11}^{\rm un}$ $\times\exp(-2(\Delta+\delta\mu)/T)$	$R_{cc,dd}\sim R_{11}^{\rm un}\exp^{-\Delta/T}$	
η	$\eta\propto\mu^5/g^3T^2$	$\eta\sim\eta_1^{\rm un}e^{-\Delta/T}$, $(\Delta/T<4)$ $\eta\sim 2\eta_1^{\rm un},(\Delta/T\gtrsim 4)$	$\eta\sim 2\eta_1^{\rm un},(\delta\mu-\Delta\gg T)$	$\eta\sim 2\eta_1^{\rm un}$	$\eta\sim 10^{-2}\eta_1^{\rm run}$
Parameters		$\frac{T}{\mu}=3.34\times10^{-4}$	$\frac{T}{\mu}=3.34\times10^{-4}$, $\frac{\Delta}{T}=2.5$	$\frac{T}{\mu}=3.34\times10^{-4}$, $\frac{\Delta_0}{\mu}=1.67\times10^{-2}$	
				$b=\zeta\delta\mu$	Like Debye
Energy scales	$\mu\gg T$	$\Delta\gg T$	a, b gapless, c, d gapped, $(\delta\mu>\Delta)$	a, b gapless, $(\delta\mu_{\rm eff}(\theta)>\Delta)$	
	a, b, c, d unpaired	a, b, c, d gapped	a, b, c, d gapped, $(\Delta>\delta\mu)$	a, b, c, d gapped, $(\lvert\delta\mu_{\rm eff}(\theta)\rvert<\Delta)$	
				c, d gapless, $(-\Delta>\delta\mu_{\rm eff}(\theta))$	Like Debye

superfluids is dominated by fermionic modes near the gapless surfaces and the result for the total viscosity in the limit $\delta\mu - \Delta \gg T$ is the same as for an unpaired system,

$$\eta(\delta\mu \gg \Delta) = \sum_i \eta_i \approx \eta_a + \eta_b \approx 2\eta_1^{\rm un}. \tag{E24}$$

The contribution from the gapped branches can be ignored,

$$\eta_c = \eta_d \approx 0. \tag{E25}$$

This somewhat complicated analysis leads to a simple and intuitive result summarized in Eq. (E24): One could restrict to modes near the gapless spheres like mode a near $\xi = -\sqrt{\delta\mu^2 - \Delta^2}$ and mode b near $\xi = +\sqrt{\delta\mu^2 - \Delta^2}$ and neglect modes c and d. Near the gapless ξ, the dispersion of the modes can be approximated as linear, which means that standard Fermi liquid techniques would lead to Eq. (E24) for gapless fermions if $\delta\mu \gg \Delta$.

This intuitive understanding helps us understand the results of the more complicated calculation for the FF phase where the pairing pattern is anisotropic in Sec. IV.

To summarize all the discussions on different types of phases here we insert a table. The table presents characteristic features of different phases in a concise manner. To summarize all the discussions on different types of phases here we insert a table (Table II)

APPENDIX F: NUMERICAL DETAILS

In this section we present some useful details of numerical integration.

The evaluation of the lhs of the Boltzmann equation [Eq. (10)] is straightforward. For $\Delta = 0, \delta\mu = 0, b = 0$ the integral can be performed analytically for $T \ll \mu$ [29,56] and gives $L^{\rm un}$ [Eq. (E2)]. For generic $\Delta, \delta\mu, b$ one can use Azimuthal symmetry to write the integral as a two-dimensional integral which can be evaluated easily numerically.

The general evaluation of the collision integral R_{ij} is more difficult. For $b = 0$, spherical symmetry can be used to simplify the integral [29,56]. The five-dimensional integration can be done easily using Monte Carlo techniques and we find converged answers with 10^5–10^6 points. The results for R_{ij} shown in Figs. 8 and 10 are obtained using 10^6 points. The error bars are the estimated errors obtained in the Monte Carlo integration. More points are required for the Landau damped exchange bosons since the $\overline{|\mathcal{M}|^2}$ and hence the integrand is more sharply peaked at $\mathbf{q} \to 0$.

For the anisotropic system ($b \neq 0$) one has to perform seven-dimensional integration instead of 5. Because of the higher dimensions the convergence of the Monte Carlo evaluation of Eq. (B7) is much slower compared to Eq. (B2). In making Fig. 3 where the mediator is Debye screened, we used 7×10^7 points and obtained reasonably converged results. The evaluation of R_{ij} for Figs. 4 and 5 was more computationally involved because the dispersions as well as the interactions are anisotropic and the interactions are mediated by Landau damped gluons. Thus the integrand is sharply peaked at small q. To evaluate R_{ij} for Fig. 4 we used 2.2×10^8 to 3.7×10^8 Monte Carlo points which took over two weeks on a modern cluster with 100 nodes. For Fig. 5, we uniformly took 2.2×10^8 points for all the four T/μ values.

The most challenging part of the computation is simultaneous solution for the energy conservation constraint $E_{p_3} - E_{p_i} = \omega = E_{p_2} - E_{p_4}$ and it required writing a robust solver in language C. The convergence of R_{ij} is poor, as seen by the large error bars in R_{ij} and η. Substantial improvements would require significantly higher computing resources and/or a better algorithm which we leave for the future.

[1] D. Page and S. Reddy, Annu. Rev. Nucl. Part. Sci. **56**, 327 (2006).
[2] F. Ozel and P. Freire, Annu. Rev. Astron. Astrophys. **54**, 401 (2016).
[3] A. Y. Potekhin, Phys. Usp. **53**, 1235 (2010).
[4] J. M. Lattimer, Annu. Rev. Nucl. Part. Sci. **62**, 485 (2012).
[5] M. Prakash, Pramana J. Phys. **84**, 927 (2015).
[6] M. G. Alford and K. Schwenzer, Phys. Rev. Lett. **113**, 251102 (2014).
[7] N. Andersson, Astrophys. J. **502**, 708 (1998).
[8] N. Andersson and K. D. Kokkotas, Mon. Not. R. Astron. Soc. **299**, 1059 (1998).
[9] L. Lindblom, J. E. Tohline, and M. Vallisneri, Phys. Rev. Lett. **86**, 1152 (2001).
[10] M. G. Alford, S. Mahmoodifar, and K. Schwenzer, Phys. Rev. D **85**, 044051 (2012).
[11] E. Flowers and N. Itoh, Astrophys. J. **206**, 218 (1976).
[12] E. Flowers and N. Itoh, Astrophys. J. **230**, 847 (1979).
[13] N. Andersson, D. I. Jones, K. D. Kokkotas, and N. Stergioulas, Astrophys. J. **534**, L75 (2000); *ICTP* Lect. Notes Ser. Vol. 3 (2001), pp. 297-314.
[14] L. Bildsten and G. Ushomirsky, Astrophys. J. **529**, L33 (2000).
[15] P. Jaikumar, G. Rupak, and A. W. Steiner, Phys. Rev. D **78**, 123007 (2008).

[16] Y. Levin and G. Ushomirsky, Mon. Not. R. Astron. Soc. **324**, 917 (2001).
[17] L. Lindblom, B. J. Owen, and G. Ushomirsky, Phys. Rev. D **62**, 084030 (2000).
[18] G. Rupak and P. Jaikumar, Phys. Rev. C **88**, 065801 (2013).
[19] L. Lindblom and G. Mendell, Phys. Rev. D **61**, 104003 (2000).
[20] L. Lindblom and B. J. Owen, Phys. Rev. D **65**, 063006 (2002).
[21] P. Haensel, K. P. Levenfish, and D. G. Yakovlev, Astron. Astrophys. **357**, 1157 (2000).
[22] P. Haensel, K. P. Levenfish, and D. G. Yakovlev, Astron. Astrophys. **372**, 130 (2001).
[23] P. Haensel, K. P. Levenfish, and D. G. Yakovlev, Astron. Astrophys. **381**, 1080 (2002).
[24] P. S. Shternin and D. G. Yakovlev, Phys. Rev. D **78**, 063006 (2008).
[25] B. Haskell and N. Andersson, Mon. Not. R. Astron. Soc. **408**, 1897 (2010).
[26] C. Manuel and L. Tolos, Phys. Rev. D **88**, 043001 (2013).
[27] G. Colucci, M. Mannarelli, and C. Manuel, Astrophys. J. **56**, 104 (2013).
[28] J. Madsen, Phys. Rev. D **46**, 3290 (1992).
[29] H. Heiselberg and C. Pethick, Phys. Rev. D **48**, 2916 (1993).
[30] K. Schwenzer, arXiv:1212.5242.
[31] K. Rajagopal and F. Wilczek, in *At the Frontier of Particle Physics*, edited by M. Shifman, Vol. 3, pp. 2061–2151.
[32] M. G. Alford, J. A. Bowers, and K. Rajagopal, J. Phys. G **27**, 541 (2001); Lect. Notes Phys. **578**, 235 (2001).
[33] M. G. Alford, A. Schmitt, K. Rajagopal, and T. Schäfer, Rev. Mod. Phys. **80**, 1455 (2008).
[34] M. G. Alford, K. Rajagopal, and F. Wilczek, Nucl. Phys. **B537**, 443 (1999).
[35] C. Manuel, A. Dobado, and F. J. Llanes-Estrada, J. High Energy Phys. 09 (2005) 076.
[36] M. Mannarelli, C. Manuel, and B. A. Sa'd, Phys. Rev. Lett. **101**, 241101 (2008).
[37] G. Rupak and P. Jaikumar, Phys. Rev. C **82**, 055806 (2010).
[38] M. G. Alford and S. Han, Eur. Phys. J. A **52**, 62 (2016).
[39] M. G. Alford, J. A. Bowers, and K. Rajagopal, Phys. Rev. D **63**, 074016 (2001).
[40] R. Anglani, R. Casalbuoni, M. Ciminale, N. Ippolito, R. Gatto, M. Mannarelli, and M. Ruggieri, Rev. Mod. Phys. **86**, 509 (2014).
[41] K. Rajagopal and R. Sharma, Phys. Rev. D **74**, 094019 (2006).
[42] N. D. Ippolito, G. Nardulli, and M. Ruggieri, J. High Energy Phys. 04 (2007) 036.
[43] X.-G. Huang and A. Sedrakian, Phys. Rev. D **82**, 045029 (2010).
[44] G. Cao, L. He, and P. Zhuang, Phys. Rev. D **91**, 114021 (2015).
[45] M. G. Alford, K. Rajagopal, and F. Wilczek, Phys. Lett. B **422**, 247 (1998).
[46] R. Rapp, T. Schäfer, E. V. Shuryak, and M. Velkovsky, Phys. Rev. Lett. **81**, 53 (1998).
[47] A. Sedrakian and D. H. Rischke, Phys. Rev. D **80**, 074022 (2009).
[48] P. Fulde and R. Ferrell, Phys. Rev. **135**, A550 (1964).
[49] A. Larkin and Y. N. Ovchinnikov, Zh. Eksp. Teor. Fiz. **47**, 1136 (1964).
[50] M. Mannarelli, K. Rajagopal, and R. Sharma, Phys. Rev. D **76**, 074026 (2007).
[51] L.-M. Lin, Phys. Rev. D **76**, 081502 (2007).
[52] B. Haskell, N. Andersson, D. I. Jones, and L. Samuelsson, Phys. Rev. Lett. **99**, 231101 (2007).
[53] B. Knippel and A. Sedrakian, Phys. Rev. D **79**, 083007 (2009).
[54] R. Anglani, G. Nardulli, M. Ruggieri, and M. Mannarelli, Phys. Rev. D **74**, 074005 (2006).
[55] D. Hess and A. Sedrakian, Phys. Rev. D **84**, 063015 (2011).
[56] M. G. Alford, H. Nishimura, and A. Sedrakian, Phys. Rev. C **90**, 055205 (2014).
[57] M. G. Alford, J. Berges, and K. Rajagopal, Nucl. Phys. **B571**, 269 (2000).
[58] D. H. Rischke, Phys. Rev. D **62**, 034007 (2000).
[59] D. H. Rischke, D. T. Son, and M. A. Stephanov, Phys. Rev. Lett. **87**, 062001 (2001).
[60] D. H. Rischke and I. A. Shovkovy, Phys. Rev. D **66**, 054019 (2002).
[61] R. Sharma, Eur. Phys. J. A **53**, 63 (2017).
[62] M. E. Peskin and D. V. Schroeder, *An Introduction to Quantum Field Theory* (Westview, Boulder, CO, 1995), including exercises.
[63] G. Baym, H. Monien, C. J. Pethick, and D. G. Ravenhall, Phys. Rev. Lett. **64**, 1867 (1990).
[64] D. T. Son and M. A. Stephanov, Phys. Rev. D **61**, 074012 (2000).
[65] D. T. Son and M. A. Stephanov, Phys. Rev. D **62**, 059902 (2000).
[66] R. Casalbuoni and R. Gatto, Phys. Lett. B **469**, 213 (1999).
[67] M. Rho, A. Wirzba, and I. Zahed, Phys. Lett. B **473**, 126 (2000).
[68] D. K. Hong, T. Lee, and D.-P. Min, Phys. Lett. B **477**, 137 (2000).
[69] C. Manuel and M. H. G. Tytgat, Phys. Lett. B **479**, 190 (2000).
[70] M. Rho, E. V. Shuryak, A. Wirzba, and I. Zahed, Nucl. Phys. **A676**, 273 (2000).
[71] M. G. Alford, J. Berges, and K. Rajagopal, Nucl. Phys. **B558**, 219 (1999).
[72] J. A. Bowers, Ph.D. thesis, MIT, LNS, 2003.
[73] J. Kundu and K. Rajagopal, Phys. Rev. D **65**, 094022 (2002).
[74] J. A. Bowers and K. Rajagopal, Phys. Rev. D **66**, 065002 (2002).
[75] M. Mannarelli, K. Rajagopal, and R. Sharma, Phys. Rev. D **73**, 114012 (2006).
[76] A. K. Leibovich, K. Rajagopal, and E. Shuster, Phys. Rev. D **64**, 094005 (2001).
[77] R. Casalbuoni, R. Gatto, N. Ippolito, G. Nardulli, and M. Ruggieri, Phys. Lett. B **627**, 89 (2005); **634**, 565(E) (2006).
[78] I. Shovkovy and M. Huang, Phys. Lett. B **564**, 205 (2003).
[79] H. Abuki and T. Kunihiro, Nucl. Phys. **A768**, 118 (2006).
[80] S. B. Ruester, V. Werth, M. Buballa, I. A. Shovkovy, and D. H. Rischke, Phys. Rev. D **72**, 034004 (2005).

[81] M. Alford and K. Rajagopal, J. High Energy Phys. 06 (2002) 031.
[82] A. W. Steiner, S. Reddy, and M. Prakash, Phys. Rev. D **66**, 094007 (2002).
[83] M. Huang and I. Shovkovy, Nucl. Phys. **A729**, 835 (2003).
[84] M. G. Alford and A. Schmitt, J. Phys. G **34**, 67 (2007).
[85] N. Iwamoto, Ann. Phys. (N.Y.) **141**, 1 (1982).
[86] N. Bogoliubov, Sov. Phys. JETP **7**, 51 (1958).
[87] I. Giannakis and H.-C. Ren, Phys. Lett. B **611**, 137 (2005).
[88] I. Giannakis and H.-C. Ren, Nucl. Phys. **B723**, 255 (2005).
[89] M. Ciminale, G. Nardulli, M. Ruggieri, and R. Gatto, Phys. Lett. B **636**, 317 (2006).
[90] R. Casalbuoni, E. Fabiano, R. Gatto, M. Mannarelli, and G. Nardulli, Phys. Rev. D **66**, 094006 (2002).
[91] R. Casalbuoni, R. Gatto, M. Mannarelli, and G. Nardulli, Phys. Lett. B **511**, 218 (2001).
[92] L. Radzihovsky and A. Vishwanath, Phys. Rev. Lett. **103**, 010404 (2009).
[93] E. Adams, J. Phys. Chem. Solids **15**, 359 (1960).
[94] J. Schrieffer, *Theory of Superconductivity*, Advanced Book Program Series (Advanced Book Program, Perseus Books, 1983).
[95] M. Alford, P. Jotwani, C. Kouvaris, J. Kundu, and K. Rajagopal, Phys. Rev. D **71**, 114011 (2005).
[96] L. Landau and I. Khalatnikov, Zh. Eksp. Teor. Fiz. **19**, 637 (1949).
[97] H. J. Maris, Phys. Rev. A **8**, 1980 (1973).
[98] G. Rupak and T. Schäfer, Phys. Rev. A **76**, 053607 (2007).
[99] C. Manuel and L. Tolos, Phys. Rev. D **84**, 123007 (2011).
[100] D. N. Aguilera, V. Cirigliano, J. A. Pons, S. Reddy, and R. Sharma, Phys. Rev. Lett. **102**, 091101 (2009).
[101] P. S. Shternin and D. G. Yakovlev, Phys. Rev. D **75**, 103004 (2007).
[102] M. Alford, C. Kouvaris, and K. Rajagopal, Phys. Rev. D **71**, 054009 (2005).